T.R.
SAKARYA UNIVERSITY
GRADUATE SCHOOL OF NATURAL AND APPLIED SCIENCES

THE EFFECT OF INCLINATION ANGLE IN FIXED PHOTOVOLTAIC SYSTEM APPLICATIONS

MSc THESIS

Abdalaziz TAREK ABDALAZIZ EBRAHEEM RAGAB

Electrical And Electronics Engineering Department

JUNE 2025

T.R.
SAKARYA UNIVERSITY
GRADUATE SCHOOL OF NATURAL AND APPLIED SCIENCES

THE EFFECT OF INCLINATION ANGLE IN FIXED PHOTOVOLTAIC SYSTEM APPLICATIONS

MSc THESIS

Abdalaziz TAREK ABDALAZIZ EBRAHEEM RAGAB

Electrical And Electronics Engineering Department

Thesis Advisor: Prof. Dr. Cenk YAVUZ

JUNE 2025

The thesis work titled “THE EFFECT OF INCLINATION ANGLE IN FIXED PHOTOVOLTAIC SYSTEM APPLICATIONS” prepared by Abdalaziz TAREK ABDALAZIZ EBRAHEEM RAGAB was accepted by the following jury on 20/06/2025 by unanimously of votes as a MSc THESIS in Sakarya University Graduate School of Natural and Applied Sciences, Electrical and Electronics department.

Thesis Jury

Head of Jury :	**Prof. Dr. Ali Fuat BOZ** Sakarya University of Applied Sciences	.....
Jury Member :	**Prof. Dr. Cenk YAVUZ** (Advisor) Sakarya University	.....
Jury Member :	**Doç. Dr. Ceyda AKSOY TIRMIKÇI** Sakarya University	……...

STATEMENT OF COMPLIANCE WITH THE ETHICAL PRINCIPLES AND RULES

I declare that the thesis work titled "THE EFFECT OF INCLINATION ANGLE IN FIXED PHOTOVOLTAIC SYSTEM APPLICATIONS", which I have prepared in accordance with Sakarya University Graduate School of Natural and Applied Sciences regulations and Higher Education Institutions Scientific Research and Publication Ethics Directive, belongs to me, is an original work, I have acted in accordance with the regulations and directives mentioned above at all stages of my study, I did not get the innovations and results contained in the thesis from anywhere else, I duly cited the references for the works I used in my thesis, I did not submit this thesis to another scientific committee for academic purposes and to obtain a title, in accordance with the articles 9/2 and 22/2 of the Sakarya University Graduate Education and Training Regulation published in the Official Gazette dated 20.04.2016, a report was received in accordance with the criteria determined by the graduate school using the plagiarism software program to which Sakarya University is a subscriber, I accept all kinds of legal responsibility that may arise in case of a situation contrary to this statement.

(……/……/20…..)

(signature)

Abdalaziz TAREK ABDALAZIZ EBRAHEEM RAGAB

To my family and friends

ACKNOWLEDGMENTS

I would like to express my deepest gratitude to my supervisor, Prof. Dr. Cenk YAVUZ, for their invaluable guidance and unwavering support through this study.

I am also profoundly grateful to the Electrical and Electronics Engineering Department at Sakarya university for providing the resources and facilities necessary to complete this study.

Special thanks to my colleagues and friends for their encouragement, assistance, and constructive discussions.

Lastly, I extend my heartfelt appreciation to my family for their patience, understanding, and unwavering support throughout this academic journey.

Abdalaziz TAREK ABDALAZIZ EBRAHEEM RAGAB

TABLE OF CONTENTS

Page

ABBREVIATIONS

IRENA : International Renewable Energy Agency
CSP : Concentrating Solar-Thermal Power
CdTe : Cadmium telluride
CIGS : Copper Indium Gallium Selenide
CAR : Central Anatolia Region
PV : Photovoltaics
GEPA : Güneş Enerjisi Potansiyelimiz

SYMBOLS

$\mathbf{H}$	: Global Solar Radiation [kWh/ m^2 /day]
$\mathbf{H_0}$	: Extraterrestrial Solar Radiation [kWh/ m^2 /day]
$\mathbf{S}$	: Sunshine Hours [h]
$\mathbf{S_0}$	: Maximum Sunshine Hours [h]
$\boldsymbol{\omega_s}$	: Sunrise Hour Angle for Horizontal Surface [°]
$\boldsymbol{\omega_s'}$	: Sunrise Hour Angle for Tilted Surface [°]
$\boldsymbol{\omega_{ss}}$	: Sunset Hour Angle for Tilted Surface to East and West [°]
$\boldsymbol{\omega_{sr}}$	: Sunrise Hour Angle for Tilted Surface to East and West [°]
$\boldsymbol{\delta}$	: Solar Declination [°]
$\boldsymbol{\gamma}$	: Azimuth Angle [°]
$\boldsymbol{\rho}$	: The Ground Reflectivity Coefficient
$\boldsymbol{\beta}$	: Tilt Angle [°]
$\boldsymbol{\phi}$	: Latitude [°]
$\mathbf{R_b}$	: Tilt Coefficient for the Beam Solar Radiation
$\mathbf{R_d}$	: Tilt Coefficient for the Diffuse Solar Radiation
$\mathbf{k_t}$	: Clearness Index
$\mathbf{k_d}$	: Diffuse Fraction
$\mathbf{k_{dd}}$	: Diffuse Coefficient
$\mathbf{H_t}$	: Total Solar Radiation for Inclined Surface [kWh/ m^2 /day]
$\mathbf{H_d}$	: Diffuse Solar Radiation [kWh/ m^2 /day]
$\mathbf{H_b}$	: Beam Solar Radiation [kWh/ m^2 /day]
$\mathbf{G_{sc}}$	: Solar Constant [1360.8 W/m^2]
$\mathbf{E}$	: Relative Percentage Error [%]
$\mathbf{R^2}$	: Coefficient of Determination
MPE	: Mean Percentage Error [%]
RSE	: Relative Standard Error
SSRE	: Sum of the Squares of Relative Errors
RMSE	: Root Mean Square Error [kWh/m^2]
MBE	: Mean Bias Error [kWh/m^2]
MAPE	: Mean Absolute Percentage Error [%]

LIST OF TABLES

Page

LIST OF FIGURES

Page

THE EFFECT OF INCLINATION ANGLE IN FIXED PHOTOVOLTAIC SYSTEM APPLICATIONS

SUMMARY

Solar energy is a clean and renewable source of energy that can help reduce our dependency on fossil fuels and solve a part of the climate change problem. As solar technology advances and becomes more affordable, it is critical to ensure that solar panel systems, such as our rooftop PV panels, operate as efficiently as possible. This study focuses on optimizing and maximizing the efficiency of the solar energy systems which built on the roof of the Electric and Electronics Engineering at Sakarya University, Turkey. Regarding the region's expanding solar potential, there is limited measured and observed data on solar irradiance and PV panels output under the impact of soiling.

The first method used to understand the effect of inclination on solar panel performance is to estimate and calculate the optimal tilt angle. This optimal angle is critical because it directly affects the quantity of solar radiation a panel can collect throughout the year. The optimum tilt angle is the angle at which a solar panel should be tilted in order to receive the most total solar energy on its surface. Achieving this optimal orientation is critical for increasing energy efficiency and maximizing the utilization of solar resources.

To determine the optimum tilt angle, it is necessary to conduct a detailed analysis of the total solar radiation incident on the panel. This involves evaluating the mathematical model of total solar radiation, which consists of three major components which are direct or beam radiation, diffuse radiation, and ground-reflected radiation. Among these, diffuse solar radiation is particularly important, especially in areas or seasons with higher cloud cover or air scatter. Unlike direct radiation, which travels in a straight line from the Sun, diffuse radiation is scattered by molecules and particles in the atmosphere and strikes the panel from many angles.

The best method to estimate the total solar radiation is to use specialized tools and sensors to take direct measurements. For every aspect of solar radiation, including diffuse radiation, these measurements offer reliable and accurate information. Unfortunately, the measurement tools are not available. Therefore, a different approach that is based on existing equations and models that through the study develop new diffuse solar radiation equations depending on pervious researches has been used. These models offer a close approximation to actual conditions because they are based on observed or computed data. The study takes a comprehensive strategy by choosing 34 models from previous studies in order to improve reliability and accuracy.

The variety of equations that estimate diffuse solar radiation under different circumstances. Give us a variety of results by computing diffused solar radiation using each model, capturing variances across various approaches and assumptions. The study calculates the average of these 34 models to further improve the estimation. Our presumed “measured value” for diffuse solar radiation in Sakarya city be this averaged

value, which presumed as measured value. To organize this, 34 equations have been divided into five distinct groups based on their characteristics, data requirements or mathematical structure. These groups help categorize the models, facilitating analysis, and enabling us to compare the performance and accuracy of different approaches. The five groups are diffuse fraction (H_d/H) calculated by clearness index (H/H_0), diffuse fraction (H_d/H) calculated by sunshine fraction (S/S_0), diffuse fraction (H_d/H)calculated by sunshine fraction (S/S_0) and clearness index (H/H_0),diffuse coefficient (H_d/H_0) calculated by clearness index (H/H_0) and diffuse coefficient (H_d/H_0) calculated by sunshine fraction (S/S_0).H_0 and S_0 are extraterrestrial solar radiation and is maximum sunshine hours respectively. Extraterrestrial solar radiation and maximum sunshine hours are the main components in our diffuse solar radiation calculation.

We have calculated monthly average daily extraterrestrial solar radiation (H_0) the availability of extraterrestrial solar radiation energy varies by month. January's give a value of 4.11 kWh/m²/day shows low solar irradiation at the start of the year. H_0 levels steadily rise over time, peaking at 7.52 kWh/m²/day in March and 5.51 kWh/m²/day in February, respectively. By April, the number increases to 9.56 kWh/m²/day, showing great solar energy potential. Solar irradiance peaks in June at 11.60 kWh/m²/day, then decreases slightly in July to 11.28 kWh/m²/day during the winter. The values continued decreasing in the second half of the year, dropping to 8.20kWh/m²/day in September and gradually decreasing to 3.68 kWh/m²/day in December. This pattern emphasizes the seasonal nature of solar energy availability, with the highest values occurring during the summer months and the lowest during winter.

The monthly average maximum sunshine hours (S_0) have calculated in this study. The results numbers show the theoretical maximum amount of daylight accessible at a specific place on a clear day. The maximum value is in June with 14.88 hours, while the lowest is in December with 9.12 hours. This variation reflects the changing length of the day caused by the Earth's axial tilt and orbit around the Sun. The data is critical for understanding seasonal variations in Sun availability. Maximum sunshine hours are affected by geographical location, particularly latitude.

After obtaining the values of extraterrestrial solar radiation and maximum sunshine hours, the next step was calculated the diffuse solar radiation using 34 models. The average value of 34 models has been used as our estimated measured value and by using MATLAB the regression methods have been applied to create our new diffuse solar radiation model for Sakarya.

In the monthly average daily of new model diffuse solar radiation, seasonal variation can be observed, with the lowest value in December (0.79 kWh/m²/day) and the highest in June (2.39 kWh/m²/day). Diffuse radiation gradually increases from winter to early summer, peaking during the sunniest months when atmospheric scattering is greatest.

By using the values of the new model diffuse solar radiation, the values have been used to calculate total solar radiation in inclined surface. In January, the average daily total solar radiation is 2.15 kWh/m²/day, and the optimum tilt angle is 57.16 degrees. During February, the solar radiation increases to 3.20 kWh/m²/day with an optimum tilt angle of 51.04 degrees. In March, the value increases more to 3.86 kWh/m²/day at a tilt angle of 36.94 degrees. By April, the average daily solar radiation reaches 4.63 kWh/m²/day with an optimum tilt angle of 20.83 degrees. The highest solar radiation

occurs in June at 6.01 kWh/m²/day with a minimal tilt angle of only 0.10 degrees. After June, the values begin to decrease gradually; for instance, in July it is 5.85 kWh/m²/day at 3.19 degrees, and August records 5.44 kWh/m²/day at 16.65 degrees. In September, it is 4.81 kWh/m²/day with an optimum tilt angle of 33.47 degrees. October sees it decrease to 3.91 kWh/m²/day at 48.65 degrees, and November drops further to 2.61 kWh/m²/day at 57.20 degrees. Finally, December has the lowest solar radiation at 2.10 kWh/m²/day with the steepest tilt angle of 60.42 degrees.

The yearly average optimum tilt angle is 32.64 degrees. Using PV*SOL, PV imulation software, it shows that the optimal tilt angle for a panel facing south throughout the year is 32 degrees. The optimum tilt angle for east and west-facing panels is from 8 to 9 degrees. This result is very similar to our determined optimum tilt angle of 32.64 degrees, showing a significant agreement between simulation results and our analytical approach. According to the PV*SOL software the PV system exports energy to the grid with a value of 5660 kWh/Year. The comparison between PV*SOL simulation results and real site measurements shows a similar pattern throughout the year. The smallest errors appear in May and June with about 0.34% difference, showing very close agreement. The largest differences occur in February with a 52.13% error and in December with a 29.94% error. The highest energy production happens in summer months like June, July, and August, which is expected due to stronger sunlight. Overall, PV*SOL provides reliable results with a total error of just 0.68%. A comparison between south, east, west, and horizontal panels based on real site data shows that east and west-facing panels can produce similar energy to horizontal panels. In some months, east and west-facing panels can even produce more than horizontal panels. This means east or west-facing panels with a small tilt like 8° to 9° as PV*SOL suggested or even the east and west site facing panels in the site can be a better choice than flat ones, as they need less cleaning efforts and cost less to maintain.PV*SOL shows that the panels facing south produced the best results between different orientations and horizontal panels. South oriented panels received the most Sun radiation with 1645.69 kWh/m², had the best performance ratio 82.56%, and produced the most electricity in a year 1632.53 kWh yearly. Zero degrees tilt angle generates 1421.22 kWh of energy each year, with a specific output of 1184.35 kWh/kWp. East-facing panels produced a little less energy than flat panels, with 1371.92 kWh/year, 1143.27 kWh/kWp, and an 81.90% performance ratio. The west-facing panels produced the lowest results. They produced only 1234.60 kWh per year and the lowest performance ratio of 79.89%. These findings indicate that orienting panels to the south is the greatest option for capturing the most energy from the Sun.

An experiment in Istanbul indicated that uncleaned panels lost approximately 0.4% of their power after 3 days, but up to 3.0% after 24 days without rain, in our PV roof system, the tilt angle of the panels has a considerable impact on decreasing soiling. Horizontal panels tend to collect more dust and have a slower snow-melting rate, increasing the amount of effort to clean. The panels set at an appropriate tilt angle require less care, especially as Sakarya sees heavy rains from November to May, which naturally helps keep the panels cleaner. However, during the summer, all panels require a regular cleaning routine to reduce the impacts of soiling.

SABİT FOTOVOLTAİK SİSTEM UYGULAMALARINDA EĞİM AÇISININ ETKİSİ

ÖZET

Güneş enerjisi, fosil yakıtlara olan bağımlılığımızı azaltmamıza ve iklim değişikliği sorununun bir kısmını çözmemize yardımcı olabilecek temiz ve yenilenebilir bir enerji kaynağıdır. Güneş teknolojisi ilerledikçe ve daha uygun fiyatlı hale geldikçe, çatı PV panelleri gibi güneş paneli sistemlerinin mümkün olduğunca verimli çalışmasını sağlamak kritik önem taşımaktadır. Bu çalışma, Türkiye'deki Sakarya Üniversitesi Elektrik ve Elektronik Mühendisliği çatısına inşa edilen güneş enerjisi sistemi gibi sistemlerin verimliliğini optimize etmeye ve en üst düzeye çıkarmaya odaklanmaktadır. Bölgenin genişleyen güneş potansiyeli ile ilgili olarak, kirlenmenin etkisi altında güneş ışınımı ve PV panellerinin çıktısı hakkında sınırlı ölçülmüş ve gözlemlenmiş veri bulunmaktadır.

Güneş paneli performansında eğimin etkisini anlamak için kullanabilecek ilk yöntem, optimum eğim açısını tahmin etmek ve hesaplamaktır. Bu optimum açı kritiktir çünkü bir panelin yıl boyunca toplayabileceği güneş radyasyonu miktarını doğrudan etkiler. Optimum eğim açısı, bir güneş panelinin yüzeyinde en fazla toplam güneş enerjisini alabilmesi için eğilmesi gereken açıdır. Bu optimum yönelime ulaşmak, enerji verimliliğini artırmak ve güneş kaynaklarının kullanımını en üst düzeye çıkarmak için kritik öneme sahiptir.

Optimum eğim açısını belirlemek için, panele gelen toplam güneş radyasyonunun ayrıntılı bir analizini yapmak gerekir. Bu, doğrudan veya ışın radyasyonu, dağınık radyasyon ve yerden yansıyan radyasyon olmak üzere üç ana bileşenden oluşan toplam güneş radyasyonunun matematiksel modelinin değerlendirilmesini içerir. Bunlar arasında, dağınık güneş radyasyonu, özellikle daha fazla bulut örtüsü veya hava saçılması olan bölgelerde veya mevsimlerde özellikle önemlidir. Güneşten düz bir çizgide ilerleyen doğrudan radyasyonun aksine, dağınık radyasyon atmosferdeki moleküller ve parçacıklar tarafından saçılır ve panele birçok açıdan çarpar.

Toplam güneş radyasyonunu tahmin etmenin en iyi yöntemi, doğrudan ölçümler almak için özel araçlar ve sensörler kullanmaktır. Dağınık radyasyon dâhil olmak üzere güneş radyasyonunun her yönü için bu ölçümler güvenilir ve doğru bilgiler sunar. Bu tez çalışması kapsamında ölçüm araçlarına erişim şansı olmadığı için önceki araştırmalara dayanarak yeni dağınık güneş radyasyonu denklemleri oluşturulacak, mevcut denklemlere ve modellere dayanan farklı bir yaklaşım kullanılacaktır. Bu modeller, gözlemlenen veya hesaplanan verilere dayandıkları için gerçek koşullara yakın bir yaklaşım sunar. Güvenilirliği ve doğruluğu artırmak için önceki çalışmalardan 34 model seçerek kapsamlı bir strateji izlenmiştir.

Farklı koşullar altında dağınık güneş radyasyonunu tahmin eden çeşitli denklemler. Her modeli kullanarak dağınık güneş radyasyonunu hesaplayarak, çeşitli yaklaşımlar ve varsayımlar arasındaki farklılıkları yakalayarak çeşitli sonuçlar ortaya koymaktadır. Tahmini daha da iyileştirmek için bu 34 sonucun ortalaması hesaplanmıştır. Sakarya

şehrindeki dağınık güneş radyasyonu için varsayılan "ölçülen değer" ortalama değer olacaktır. Bunu düzenlemek için, 34 denklem özelliklerine, veri gereksinimlerine veya matematiksel yapılarına göre beş ayrı gruba ayrılmıştır. Bu gruplar modelleri kategorize etmeye, analizi kolaylaştırmaya ve farklı yaklaşımların performansını ve doğruluğunu karşılaştırmaya yardımcı olur. Beş grup, berraklık indeksi (H/ H0) ile hesaplanan dağınık kesir (Hd/H), güneşlenme kesri (S/S0), ile hesaplanan dağınık kesir (Hd/H), güneşlenme kesri (S/S0) ve berraklık indeksi (H/ H0), ile hesaplanan dağınık kesir (Hd/H), berraklık indeksi (H/ H0) ile hesaplanan dağınık katsayı (Hd/H0) ve güneşlenme kesri (S/S0) ile hesaplanan dağınık katsayı (Hd/H0) 'dır. H0 ve S0 sırasıyla dünya dışı güneş radyasyonu ve maksimum güneşlenme saatidir. Dünya dışı güneş radyasyonu ve maksimum güneşlenme saati, dağınık güneş radyasyonu hesaplamadaki ana bileşenlerdir.

Aylık ortalama günlük dünya dışı güneş radyasyonu H0 hesaplanmıştır, dünya dışı güneş radyasyonu enerjisinin mevcudiyeti aydan aya değişmektedir. Ocak ayı 4.11 kWh/m²/gün değerini verir, yılın başında düşük güneş ışınımı olduğunu gösterir. H_0 seviyeleri zamanla istikrarlı bir şekilde yükselerek sırasıyla Mart ayında 7.52 kWh/m²/gün ve Şubat ayında 5.51 kWh/m²/gün ile zirveye ulaşır. Nisan ayına gelindiğinde, sayı 9.56 kWh/m²/gün'e çıkarak büyük bir güneş enerjisi potansiyeli gösterir. Güneş ışınımı Haziran ayında 11.60 kWh/m²/gün ile zirveye ulaşır, ardından Temmuz ayında hafifçe düşerek kışın 11.28 kWh/m²/gün'e iner. Değerler yılın ikinci yarısında azalmaya devam ederek Eylül ayında 8.20 kWh/m²/gün'e ve Aralık ayında kademeli olarak 3.68 kWh/m²/gün'e düşer. Bu model, güneş enerjisi mevcudiyetinin mevsimsel yapısını vurgular; en yüksek değerler yaz aylarında, en düşük değerler ise kış aylarında görülür.

Aylık ortalama maksimum güneş ışığı saatleri S0 hesaplanmıştır. Sonuçlar, açık bir günde belirli bir yerde erişilebilen teorik maksimum gün ışığı miktarını gösterir. Maksimum değer 14.88 saatle Haziran ayındayken, en düşük değer 9.12 saatle Aralık ayındadır. Bu değişim, Dünya'nın eksen eğikliği ve Güneş etrafındaki yörüngesinden kaynaklanan değişen gün uzunluğunu yansıtır. Veriler, güneş bulunabilirliğindeki mevsimsel değişimleri anlamak için kritik öneme sahiptir. Maksimum güneş ışığı saatleri coğrafi konumdan, özellikle enlemden etkilenir.

Dünya dışı güneş radyasyonu ve güneşlenme süresi değerlerini elde ettikten sonra, 34 model kullanarak dağınık güneş radyasyonu hesaplanmıştır. 34 modelin ortalama değeri tahmini ölçülen değer olarak kullanılmış ve MATLAB kullanarak Sakarya için yeni dağınık güneş radyasyonu modelini oluşturmak için regresyon yöntemleri uygulanmıştır. Model dağınık güneş radyasyonunun aylık ortalama günlük değişimlerini vermektedir, en düşük değer Aralık ayında (0.79 kWh/m²/gün) ve en yüksek değer Haziran ayında (2.39 kWh/m²/gün) olmak üzere mevsimsel değişim gözlemlenebilir. Dağınık radyasyon, kıştan yaz başına doğru kademeli olarak artar ve atmosferik saçılmanın en fazla olduğu en güneşli aylarda zirveye ulaşır.

Yeni model dağınık güneş ışınımının değerleri dikkate alınarak, bu değerler eğimli yüzeydeki toplam güneş ışınımını hesaplamak için kullanılmıştır. Ocak ayında, ortalama günlük toplam güneş ışınımı 2.15 kWh/m²/gündür ve optimum eğim açısı 57.16 derecedir. Şubat ayında, güneş ışınımı 51.04 derecelik optimum eğim açısıyla 3.20 kWh/m²/güne yükselir. Mart ayında, değer 36.94 derecelik eğim açısıyla 3.86 kWh/m²/güne daha da artar. Nisan ayında, ortalama günlük güneş ışınımı 20.83 derecelik optimum eğim açısıyla 4.63 kWh/m²/güne ulaşır. En yüksek güneş ışınımı, sadece 0.10 derecelik minimum eğim açısıyla Haziran ayında 6.01 kWh/m²/gün olarak

gerçekleşir. Haziran ayından sonra değerler kademeli olarak azalmaya başlar; örneğin, Temmuz ayında 3.19 derecede 5.85 kWh/m²/gün, Ağustos ayında ise 16.65 derecede 5.44 kWh/m²/gün kaydedilir. Eylül ayında 33.47 derecelik optimum eğim açısıyla 4.81 kWh/m²/gündür. Ekim ayında 48.65 derecede 3.91 kWh/m²/güne düşer ve Kasım ayında 57.20 derecede 2.61 kWh/m²/güne düşer. Son olarak, Aralık ayında 60.42 derecelik en dik eğim açısıyla 2.10 kWh/m²/gün ile en düşük güneş radyasyonu vardır. Yıllık ortalama optimum eğim açısı 32.64 derecedir.

Yıllık ortalama optimum eğim açısı 32,64° olarak belirlenmiştir. PV simülasyon yazılımı olan PVSOL kullanılarak yapılan analizlerde, yıl boyunca güneye bakan paneller için optimum eğim açısının 32° olduğu, doğu ve batı yönelimli paneller için ise optimum eğim açısının 8° ile 9° arasında değiştiği görülmüştür. Bu sonuç, tarafımızca analitik olarak belirlenen 32,64°'lik optimum eğim açısıyla oldukça uyumlu olup, simülasyon sonuçları ile hesaplamalarımız arasında anlamlı bir örtüşme olduğunu göstermektedir. PVSOL yazılımına göre, PV sistemi yıllık bazda şebekeye 5660 kWh enerji vermektedir. PVSOL simülasyon sonuçları ile saha ölçümleri karşılaştırıldığında, yıl boyunca benzer bir eğilim izlendiği görülmektedir. En düşük hata oranları Mayıs ve Haziran aylarında yaklaşık %0,34 fark ile elde edilmiş olup, oldukça yakın sonuçlar sunmaktadır. En yüksek hata oranları ise Şubat ayında %52,13 ve Aralık ayında %29,94 olarak gözlemlenmiştir. En yüksek enerji üretimi ise beklendiği üzere Haziran, Temmuz ve Ağustos gibi yaz aylarında gerçekleşmiştir. Genel olarak PVSOL yazılımı, %0,68 gibi oldukça düşük bir toplam hata oranıyla güvenilir sonuçlar sağlamaktadır. Gerçek saha verilerine dayalı olarak yapılan güney, doğu, batı ve yatay panel karşılaştırmasında, doğu ve batı yönelimli panellerin yatay panellere benzer miktarda enerji üretebildiği, bazı aylarda ise yatay panellerden daha yüksek üretim değerlerine ulaşabildiği tespit edilmiştir. Bu durum, PV*SOL yazılımının önerdiği gibi 8° ile 9° arasında küçük bir eğime sahip doğu veya batı yönelimli panellerin ya da mevcut sitedeki doğu ve batı yönelimli panellerin, düz yerleştirilen panellere kıyasla daha avantajlı bir seçenek olabileceğini göstermektedir. Ayrıca bu panellerin daha az temizlik gerektirmesi ve bakım maliyetlerinin daha düşük olması da uzun vadede ek bir avantaj sağlamaktadır.

PVSOL, güneye bakan panellerin farklı yönelimler ve yatay paneller arasında en iyi sonuçları ürettiğini göstermektedir. Güney yönelimli paneller 1645.69 kWh/m² ile en fazla güneş ışınımını almış, %82.56 ile en iyi performans oranına sahip olmuş ve yılda en fazla elektriği 1632.53 kWh üretmiştir. Sıfır derece eğim açısı her yıl 1421.22 kWh enerji üretirken, özgül çıktısı 1184,35 kWh/kWp'dir. Doğuya bakan paneller düz panellerden biraz daha az enerji üretmiştir; sırasıyla 1371.92 kWh/yıl, 1143.27 kWh/kWp ve %81.90 performans oranına sahiptir. Batıya bakan paneller en düşük sonuçları üretmiştir. Yılda sadece 1234.60 kWh ve %79.89'luk en düşük performans oranını üretmişlerdir. Bu bulgular, panellerin güneye yönlendirilmesinin güneşten en fazla enerjiyi yakalamak için en iyi seçenek olduğunu göstermektedir.

İstanbul'da yapılan bir deney, temizlenmemiş panellerin 3 gün sonra güçlerinin yaklaşık %0.4'ünü kaybettiğini, ancak yağmursuz geçen 24 günün ardından %3.0'a kadar güç kaybettiğini göstermektedir. PV çatı sisteminde, panellerin eğim açısı kirlenmeyi azaltmada önemli bir etkiye sahiptir. Yatay paneller daha fazla toz toplama eğilimindedir ve daha yavaş bir kar erime hızına sahiptir, bu da temizleme

gerksinimini artırır. Uygun bir eğim açısına ayarlanan paneller daha az bakım gerektirir, özellikle Sakarya'da Kasım'dan Mayıs'a kadar yoğun yağışlar görüldüğünden, bu da panellerin doğal olarak daha temiz kalmasına yardımcı olur.

Ancak yaz aylarında, kirlenmenin etkilerini azaltmak için tüm paneller için düzenli bir temizlik rutini gereklidir.

1. INTRODUCTION

Solar energy is the most abundant and limitless renewable energy source on Earth. It is derived from the Sun's radiation, which can be transformed into useful energy forms like electricity and heat. The Sun emits massive amounts of energy, roughly 173000 terawatts of solar energy, which strikes the Earth on a continuous basis, which is more than 10000 times the world's entire energy consumption [1].

Photovoltaic (PV) systems turn sunlight directly into electricity, while solar thermal systems heat water or air for home, commercial, or industrial applications. Over the last few decades, advances in solar technology, combined with falling costs, have made solar power one of the world's fastest-growing energy sources. According to the International Renewable Energy Agency (IRENA), global solar photovoltaic capacity has grown from 40 gigawatts in 2010 to more than 1000 gigawatts by 2023, indicating the technology's rapid adoption [2].

1.1. History of Solar Energy

Solar energy was first discovered and used scientifically in the 19th century. After noticing that light may cause a little electric current to flow through a substance, French physicist Alexandre-Edmond Becquerel discovered the photovoltaic phenomenon in 1839. For the first time, this important finding demonstrated that sunlight could generate electricity in specific materials. The earliest prototype solar cells were constructed by inventors using selenium in the 1870s and 1880s [3].

William Adams, for instance, developed a selenium cell in 1877 with an efficiency of about 0.5%. Charles Fritts enhanced this in 1883 by covering selenium with a thin layer of gold. Then. In the meantime, the fundamental idea behind all photovoltaic systems was the theoretical explanation of how photons might free electrons from materials, which was given by Albert Einstein's theory of the photoelectric effect in 1905. Long before there were useful solar panels, these early inventions established the fundamentals of turning sunshine into power [3].

In the middle of the 20th century, significant discoveries were made. The basic structure that makes effective solar cells possible was discovered in 1939 by Russell Ohl at Bell Laboratories: the silicon p-n junction. Based on this, scientists Calvin Fuller, Gerald Pearson, and Daryl Chapin of Bell Laboratories constructed the first contemporary silicon solar cell in 1954, with an efficiency of roughly 6%. This was a turning point because it proved that solar cells could produce useful power of electricity. The earliest practical PV use was a telephone repeater in Georgia that was powered by a solar cell installed by Bell Labs around 1955. The new technology gained rapid adoption in the space field. The Soviet Sputnik three satellite quickly followed with a photovoltaic system, and the Vanguard one satellite, which had six silicon cells on board, became the first spacecraft to use solar power in 1958. Thus, a significant driving force behind the advancement of solar cells was the space race.

The application of solar energy technology progressively expanded in the decades that followed. The 1970s oil problems sparked an acceleration of interest in renewable energy. In an effort to reduce expenses, engineers started utilizing new substances and techniques as research grew. For instance, the manufacturing process changed from producing exclusively single-crystal silicon to producing cheaper polycrystalline silicon and even thin layers of amorphous silicon. The commercialization of solar cells for broader uses was spearheaded by businesses such as (SOALREX), which was established in 1973. Solar panels got cheaper and more efficient over time. Classifying solar cells into "generations" according to the materials and fabrication techniques employed became helpful as the technology advanced. The significant advancements in solar cell design and material architecture over time are reflected in this generational framework.

1.2. How Solar Energy Works

Solar energy can be transformed into electricity or heat energy using various methods. There are two fundamental approaches: photovoltaics (PV) and concentrated solar-thermal systems (CSP) [4]. Photovoltaic systems use semiconductor devices (solar cells) that convert sunlight into electricity through the photoelectric effect. When photons strike a solar cell, they excite electrons in the semiconductor and form electron-hole pairs [5]. The built-in electric field of the cell's p-n junction subsequently separates these charge carriers (electrons on one side and holes on the other),

producing an electric current and voltage. In concentrating solar power (CSP) systems, enormous arrays of mirrors or lenses direct sunlight to a receiver [5,6]. This intense light is transformed into heat, usually by heating a fluid. The thermal energy powers a heat engine, often a steam turbine, to generate electricity. PV systems convert sunshine into energy through semiconductors, while CSP uses solar heat to fuel a traditional thermal power cycle [6,7]. (Passive solar designs, such as those designed for sunshine and heat retention, use sunlight for lighting or warmth but do not actively generate power).

1.3. Generations of Photovoltaic Solar Cells

Solar photovoltaic (PV) technologies are commonly classified into three generations. First, second, and third generation. Every generation has its own advantages, disadvantages, and uses.

1.3.1. First generation of photovoltaic solar cells (crystalline silicon solar cells)

First-generation solar cells are the traditional crystalline silicon devices. These cells are made from silicon wafers and use a silicon homojunction (p-type silicon connected to n-type silicon). Because the silicon semiconductor industry was already well-established (through the microchip sector), first-generation cells made using these wafer processes dominated early solar power [3]. By 2020, crystalline silicon modules accounted for approximately 95% of global solar PV production [8]. First-generation silicon cells contain thick absorbers (100-200 μm) and reach conversion efficiencies of over 20% (with world-record laboratory devices about 26%) [9]. Monocrystalline silicon cells, manufactured from a single crystal, are generally the most efficient, whereas polycrystalline silicon (cast from several crystal grains) is less expensive but slightly less efficient [9]. These wafer-based cells are still widely used due to their maturity, stability, and large production base.

1.3.1.1. Advantages of first-generation photovoltaic solar cells

Stable performance: Reliable even under changing environmental conditions.

High efficiency: Especially monocrystalline, with lab efficiencies exceeding 25%.

Long lifespan: Often lasts more than 25 years, with slow breakdown.

1.3.1.2. Disadvantages of first-generation photovoltaic solar cells

Tough structure: Panels are often heavy and inflexible.

High manufacturing costs: Include energy-intensive silicon purification and wafer manufacture.

Material waste: Includes significant silicon loss during slicing.

1.3.2. Second generation of photovoltaic solar cells (thin-film solar cells)

Second-generation cells use less semiconductor material, reducing costs significantly. These are thin-film solar cells. Thin-film cells have a light-absorbing semiconductor layer that is only a few micrometers thick, as opposed to hundreds of micrometers. Thin films allow for a variety of manufacturing methods (such as sputtering or chemical deposition on glass, metal, or plastic substrates), as well as the production of flexible or lightweight modules. The goal was to maintain appropriate efficiency while reducing fabrication costs. Although thin film cells were initially less efficient than silicon wafers, they steadily improved and enabled faster, cheaper production. Common second-generation materials include cadmium telluride (CdTe) and copper indium gallium selenide (CIGS). These semiconductors can be deposited as very thin layers. A typical CIGS cell includes a metal backing (usually molybdenum on glass), a CIGS absorber layer, a thin CdS buffer layer, and a transparent conductive oxide front contact [9]. CdTe cells have a similar multilayer structure, with a glass substrate, transparent conductive oxide, a CdS window layer, and a CdTe absorber. Thin-film modules enabled new uses since they could be lightweight or flexible.

CIGS thin-film modules can be manufactured on flexible substrates, making them suitable for building facades, cars, and portable electronics. Cadmium telluride (CdTe) cells were the most commercially successful thin-film technology. CdTe is a direct-bandgap material (~1.5 eV) suited for solar conversion. The original prototype CdTe cell (1972) had just 6% efficiency, but advances have pushed lab CdTe cells to over 22% efficiency. CIGS technology has advanced, with current records of over 23% efficiency. In the early 21st century, thin-film cells outperformed thick silicon wafers with over 20% efficiency, reduced production costs, and faster energy payback times. Thin films sacrifice some efficiency for cost, production speed, and flexibility benefits [9-11].

1.3.2.1. Advantages of second-generation photovoltaic solar cells

Lower manufacturing Costs: Large-scale production is easier and more cost-effective.

Better low-light Performance: Works better than crystalline cells in diffused sunlight.

Flexible and lightweight: Can be applied to flexible substrates for portable or curved applications.

Lower material Use: Thin layers mean less semiconductor material is needed.

1.3.2.2. Disadvantages of second-generation photovoltaic solar cells

Lower efficiency: Compared to crystalline silicon.

Less mature technology: Means less long-term performance data and a lower market share.

Shorter lifespan: Degrades faster than first-generation PV.

Toxic materials: Some products include cadmium, which is hazardous to the environment and health.

1.3.3. Third generation photovoltaic solar cells (emerging technologies)

Third-generation solar technologies aim for higher efficiency and lower prices than first- and second-generation cells. These include multijunction (tandem) cells and new material-based cells. Multijunction cells stack multiple semiconductor layers with varying band gaps, allowing each layer to absorb a different section of the solar spectrum. For example, a stack could have gallium indium phosphide, gallium arsenide, and Germanium connections. By splitting sunlight in this manner, multijunction cells can significantly exceed the efficiency limit of a single-material cell. Theoretical simulations indicate that a perfect infinite-junction cell under focused sunlight can achieve approximately 85% efficiency [12]. Laboratory multijunction III-V solar cells achieved efficiencies of 40%, the greatest among all solar cells. Because they require expensive, high-purity materials, they are now used mostly in specialized applications such as space satellites or concentrated photovoltaic systems. The high material cost renders them unsuitable for large-area terrestrial applications. However, they hold the efficiency record for solar cells.

Another type of third-generation cell is perovskite solar cells. In 2009, a halide perovskite cell having the crystal structure, such as methylammonium lead iodide, was

shown to achieve approximately 3.8% efficiency [13]. Perovskites have an adjustable bandgap, allowing researchers to change the material's light-absorbing capabilities by changing its chemical makeup. The efficiency of perovskite cells has increased dramatically in less than a decade, reaching more than 25%. They are frequently coupled with silicon in tandem cells; for example, a perovskite-on-silicon tandem recently attained approximately 29% combined efficiency [9]. Other new approaches include organic (polymer-based) solar cells, dye-sensitized cells (which use a light-absorbing dye on a semiconductor scaffold), and quantum-dot cells. These third-generation technologies typically provide new benefits (such as low-cost fabrication or flexibility), although they are still in development. Some materials, such as perovskites, are unstable and do not have the same lifespan as silicon. Nonetheless, they demonstrate the next frontier of solar research, which seeks to combine high efficiency with low cost or innovative form factors [3].

1.3.3.1. Advantages of third-generation photovoltaic solar cells

Potential for high efficiency: Especially with tandem structures (e.g., perovskite + silicon).

Lightweight and flexible: Easily integrated into wearables or building materials.

Innovative applications: Include transparent, colourful, or flexible panels for aesthetic integration.

1.3.3.2. Disadvantages of third-generation photovoltaic solar cells

Short lifespan: Unlike standard PV, it has not yet been demonstrated to be durable over time.

Toxic elements: Some perovskites contain lead.

Not Fully Commercialized: Still in research or early-stage implementation; scalability unknown.

Stability issues: Many degrade rapidly when exposed to moisture, oxygen, or UV light.

1.4. Purpose of the Thesis

The purpose of this study is to study how inclination angle affects photovoltaic (PV) solar panels' ability to generate power, as well as how soiling and dirt effect on system

performance. To achieve this a rooftop PV solar panel system was installed on the building of the Electrical and Electronics Engineering department as a case study. Optimizing the way the system works and offering useful suggestions to increase its effectiveness are the main aims. To do this, calculate the total solar radiation in an inclined surface as well as each of its components, which are the beam (direct) and diffuse radiation, by creating a new diffuse solar radiation equation model. These calculations be used to determine the optimum tilt angle for each month of the year as well as the optimum tilt angle for the entire year. The rooftop PV system also be simulated using simulation software. Through this simulation, it is possible to analyse the energy output and efficiency of the system while taking soiling effects and tilt angle changes effects into account.

1.5. Literature Review

Sever's study estimates Turkey's monthly average, daily, and horizontal diffuse solar radiation. Strong agreement with observed data has been shown by the authors' first-order equation correlations for diffuse radiation that are based on the clearness index and relative sunshine hours. Building on earlier approaches, their work highlights the significance of location-specific characteristics for the accurate estimation of diffuse radiation. For solar energy applications, especially in areas with little data on diffuse radiation [14].

Barbaro et al [15]. Used data from three Italian stations (Palermo, Macerata, and Genova) to investigate the relationship between diffuse solar radiation, global and extraterrestrial radiation, and relative sunshine duration. The authors present empirical equations for estimating diffuse radiation, highlighting the significance of location-specific factors for greater accuracy. They use a relative standard error of estimate to assess the fit of their models, discovering that linear and quadratic equations best match experimental data in various regions. The study underlines the possibility of constructing universal relationships for diffuse radiation in places with similar meteorological characteristics, which could benefit solar energy applications.

Kaygusuz and Ayhan analyse observed solar radiation data for Trabzon, Turkey, from 1990 to 1993, concentrating on both global and diffuse radiation components. The authors provide correlation models that use statistical analysis of collected data to calculate hourly and monthly diffuse radiation. Their research focus on radiation

patterns in the Black Sea region, which is essential for constructing effective solar energy systems. The study expands on previous research while also providing new insights into the unique properties of diffuse radiation in the area [16].

This study by Aras et al [17]. focuses on developing new hybrid models to estimate monthly average daily diffuse solar radiation over Turkey's Central Anatolia Region (CAR), where such measurements are unavailable. The authors analyse and compare twenty existing models, using their predictions to calibrate twelve new hybrid models, with the best-performing model being a cubic polynomial form. The research fills an important gap in solar radiation data for the region, providing valuable information for solar energy applications. Their work contributes to improving the accuracy of diffuse solar radiation estimations, which are crucial for designing and optimizing solar energy systems. Their work contributes to improving the accuracy of diffuse solar radiation estimations, which are crucial for designing and optimizing solar energy systems.

Using three years of observed data, Elhadidy and AbdelNabi's study examines the relationship between the diffuse fraction and clearness index of daily global solar radiation in Dhahran, Saudi Arabia. The diffuse fraction is much greater in the summer than it is in the winter, according to correlations the authors created for the various seasons. Their results show that the diffuse fraction correlation is location independent and seasonal dependent, with dust notably increasing the diffuse component. While presenting new perspectives unique to Dhahran's arid climate, the findings are consistent with earlier research [18].

In addition to establishing a theoretical foundation for current empirical equations such as the Angstrom correlation, this paper by P.C. Jain creates a theoretical model for calculating diffuse and global solar irradiation on horizontal surfaces. In order to clarify the relationships between the constants that exist in different solar radiation equations, the model defines three fundamental parameters Instantaneous transmission coefficient for diffuse radiation on horizontal surface for clear sky conditions, Instantaneous transmission coefficient for diffuse radiation on horizontal surface for cloudy sky conditions and Instantaneous transmission coefficient for direct radiation for clear sky conditions that describe all of them. The theoretical approach was validated by the good connection between the calculated equations and experimental data from locations in Zimbabwe and Italy. The study creates a common paradigm for

estimating Sun irradiation and offers insightful information on diffuse radiation patterns [19].

Tarhan and Sari focuses on developing mathematical models to predict monthly average daily global and diffuse solar radiation over Turkey's Central Black Sea Region, covering five provinces. The authors developed a statistically significant quadratic polynomial model for global radiation and a hybrid model for diffuse radiation based on predictions from six existing models, as no experimental data was available. Both models were found adequate for predicting solar radiation in the region, with the hybrid model for diffuse radiation achieving very high R^2 values. The research contributes to filling the gap in solar radiation analysis for the Central Black Sea Region, providing valuable information for future engineering and scientific projects [20].

The relationship between direct and diffuse solar radiation is examined in this paper by Liu and Jordan, who also provide empirical equations for estimating diffuse radiation on horizontal surfaces in both cloudy and clear conditions. After analysing data from several places, the scientists came up with a linear connection between the transmission coefficients for diffuse and direct radiation that was generally in good agreement. Their results show that on clear days, diffuse radiation makes up about twelve percentage of extraterrestrial radiation, but on partly cloudy days, it can reach over 25 percentage, with cloudiness greatly raising diffuse radiation levels. In order to provide useful information for calculating solar radiation in regions without measurement data, the study also provides statistical distributions of daily total radiation and its relationship to monthly averages [21].

Erbs, Klein, and Duffie develop equation models for estimating the diffuse fraction of hourly, daily, and monthly-average global solar radiation using data from four U.S. locations. The authors found that the hourly diffuse fraction is strongly correlated with the clearness index (kt) and developed a relationship that accounts for seasonal variations in diffuse radiation. They also derived daily and monthly average diffuse fraction correlations, demonstrating how the statistical variation of diffuse radiation impacts solar energy system performance predictions. The results support previous findings that diffuse radiation estimation methods are generally location-independent, with some seasonal dependence observed [22].

Using experimental data from the Solar Energy Institute at Ege University, Ulgen and Hepbasli's research creates equation models to predict the monthly average daily global solar radiation for Izmir, Turkey. These models' increased accuracy can be shown by comparing them to 25 other models that are currently in use using statistical error analysis. The study divides models for estimating solar radiation into four categories: angular, linear, polynomial, and other models. Additionally, Ulgen and Hepbasli include measurements of both global and diffuse solar radiation using a pyranometer and a shadow band [23].

Ying Yu et al [24]. enhance the estimation of diffuse solar radiation by proposing an adaptive Liu and Jordan-type model that groups kt–k data points using solar elevation angle as a constraint, achieving 4–6 percentage error reduction compared to conventional all-data models. Using hourly radiation data from Shanghai, Xi'an, and Lhasa, the cubic polynomial grouping models show better accuracy under different weather circumstances, with the best performance on overcast days and during sunrise/sunset. This approach improves statistical modelling by incorporating data stratification and climatic fluctuation, hence eliminating regional constraints in diffuse fraction correlation.

Liu et al [25]. investigate the changing relationship between solar radiation and sunshine duration in Chinese cities, attributing changes to aerosol driven global dimming and brightening caused by development. Using the Angstrom model, they show that calibrating with a 10-year dataset improves accuracy, far exceeding long term calibrations influenced by non-stationary skies. The study emphasizes the necessity for improved calibration methods in fast emerging countries to account for aerosol impacts. While diffuse solar radiation is not explicitly addressed, the results improve solar resource assessment for energy applications.

Tiris et al [26]. used sunshine hours to create empirical models for global, diffuse, and beam radiation in Turkey, presenting equations that were confirmed with minimal statistical errors (MPE, RMSE), highlighting the shortage of data in specific locations.

Lingamgunta and Veziroglu proposed a universal clear sky insolation model that includes latitude and altitude, correcting previous underestimations and emphasizing altitude's role in radiation reduction [27].

Bulent Aksoy found significant errors in Turkish actinograph data and proposed a quadratic sunshine-based model with nearly 4 percent error, which outperformed actinograph reliability [28].

Muneer and Munawwar found that sunshine fraction and cloud cover were strong predictors of diffuse radiation, although air mass had little influence, recommending the use of combined parameters for accuracy across nine global sites [29].

Dincer emphasized the relevance of renewable energy in sustainable development, relating it to environmental mitigation (acid rain, ozone depletion), as well as policy integration and decentralized systems [30].

Ideriah proposed a model for direct and diffuse radiation under cloudy skies, which was validated for Ibadan with less than or equal to 15 percent error using a cloudiness coefficient and integrating King and Buckius' clear sky model [31].

Klein developed Liu and Jordan's isotropic model for vertical surfaces, which served as the foundation for later anisotropic models such as Hay's and Reindl's in building-integrated PV design [32].

Xu et al [33]. investigate the best tilt angle for filthy PV panels, concentrating on how dust deposition impacts the performance and energy output of solar systems. They present a comprehensive model that takes into account both dust accumulation and its impact on the solar irradiance received by PV panels. Their research entails collecting experimental data from different PV installations in order to validate their model. The study found that altering the tilt angle can greatly reduce the negative impacts of soiling, increasing overall energy output. According to Xu et al., making periodic tilt angle modifications depending on local climatic conditions and soiling patterns can improve the efficiency and cost- cost-effectiveness of PV systems over time.

Abdeen et al [34]. Present a complete analysis of the impacts of temperature on PV panel performance in Aswan, Egypt, showing that higher temperatures significantly affect PV system efficiency. The study contains thorough measurements of PV panel output at various tilt angles and temperature conditions, which reveal a definite inverse link between temperature and PV efficiency. In addition, the study looks into the impact of dust and soiling on PV panels, finding that dust collection exacerbates efficiency losses.

Aksoy Tirmikci presents a study that developed nine diffuse solar radiation equations for Sakarya, Turkey, by using 17 equation models from previous studies based on the clearness index, sunshine fraction. The authors apply statistical analysis of these equations to predict monthly average daily diffuse, beam, and total solar radiation, with a focus on diffuse fraction accuracy. Also, the tilt angle-total radiation equation is used to calculate the optimal tilt angles for solar panels [35]. This study develops a new diffuse solar radiation model equation for Sakarya, Turkey, by using 34 models from the previous studies that enhance to approach to values closer to reality.

2. SOLAR RADIATION

Solar radiation refers to the electromagnetic radiation emitted by the Sun [36,37]. It has a wide range of wavelengths and transports the energy that powers the Earth's climate and ecosystems. Almost all life on Earth is dependent on sunlight: it provides warmth and drives photosynthesis, the process by which plants, algae, and certain microorganisms transform light energy into chemical energy. Oxygenic photosynthesis, fueled by solar photons, produces the majority of the Earth's atmospheric oxygen and biomass [38], supporting life on Earth. Sunlight also controls the temperature by providing nearly all of the Earth's incoming energy. The Earth absorbs around 70% of incoming solar energy (the rest is deflected back into space) and reradiates this energy as heat to maintain thermal balance. Earth's normal surface temperature would be below freezing without the Sun's heating [39]. However, the natural greenhouse effect, which is maintained by solar heating of the surface and atmosphere, keeps the average surface temperature near +14 °C rather than about -18\degc\ [39]. The balance of incoming solar flux and outgoing terrestrial radiation defines Earth's energy budget [40], and even small variations in solar irradiance can impact climate.

Solar radiation is frequently measured at the top of the atmosphere. The Earth receives only one-fourth of the Sun's irradiance (340 W/m²) due to the planet's shape and the fact that half of it is dark [40]. The Sun's output to Earth varies very little over time (by about 0.1% over an 11-year sunspot cycle) [41], therefore, it was formerly known as the "solar constant." However, even minor variations in this flow can have a long-term impact on the climate.

Solar radiation (sunlight) is critical to Earth's climate and life. It generates heat that regulates weather and climate, as well as light energy for photosynthesis. Sunlight's electromagnetic spectrum contains ultraviolet (UV), visible, and infrared (IR) wavelengths. The Sun's visible light (≈400-700 nm) makes up roughly half of its output, with the remaining coming from near-UV and near-IR wavelengths. Wide-

spectrum radiation is the solar resource that supports weather, climate, and ecosystems [36].

2.1. Solar Spectrum and Its Components

The Sun emits radiation across the electromagnetic spectrum as shown in (Figure 2.1. Electromagnetic spectrum.), but most of its energy lies in three major bands: ultraviolet (UV), visible, and infrared (IR).

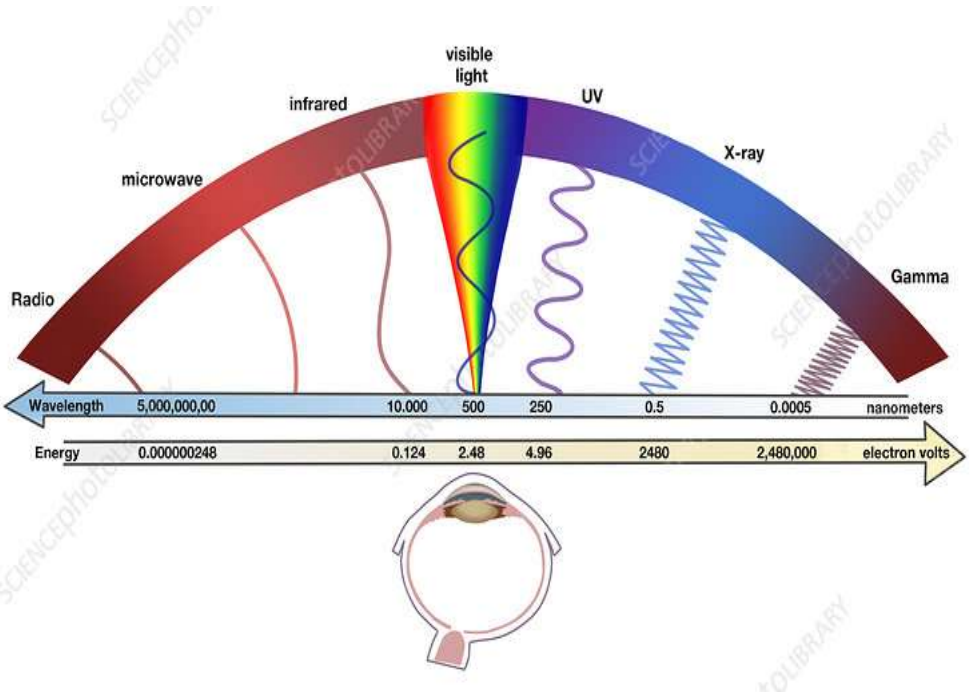

Figure 2.1. Electromagnetic spectrum [42].

The UV band (100-400 nm) is divided into UVA, UVB, and UVC; solar UV is primarily UVA (315-400 nm) and UVB (280-315 nm), with shorter UVC absorbed by the atmosphere. The human eye can detect visible light ranging from 400 to 700 nm. The infrared spectrum runs from 700 nm to millimeters range; however, the great majority of solar electricity is generated in the near-IR (700-2500 nm). Visible wavelengths account for almost half of the Sun's power [43].

The remaining energy is divided between UV and IR, with IR dominating [43]. These spectrum components are critical: visible light drives photosynthesis, UV affects air chemistry (ozone production), and infrared is principally responsible for heating. When measured above the Earth's atmosphere, the Sun's light nearly resembles that of a 5800 K blackbody. According to Wien's law, an object at this temperature generates

the most light around 500 nm (green light), which explains why the Sun appears yellow white to human eyes. Small differences from a perfect blackbody result from gas absorption in both the Sun's atmosphere and, for ground-based studies, the Earth's atmosphere.

2.2. Solar Radiation Measuring Tools

Solar radiation is measured by using equipment that captures broadband or spectral irradiance at a specific place. Common ground-based radiometers are pyranometers and pyrheliometers. A pyranometer measures global horizontal irradiance, which is the total solar power per unit area arriving on a horizontal surface from all sky directions. This includes both direct sunlight and diffuse sky radiation.

Figure 2.2. Pyranometer [44].

Pyranometers absorb and quantify all wavelengths of sunlight using a thermopile sensor placed under a glass dome.

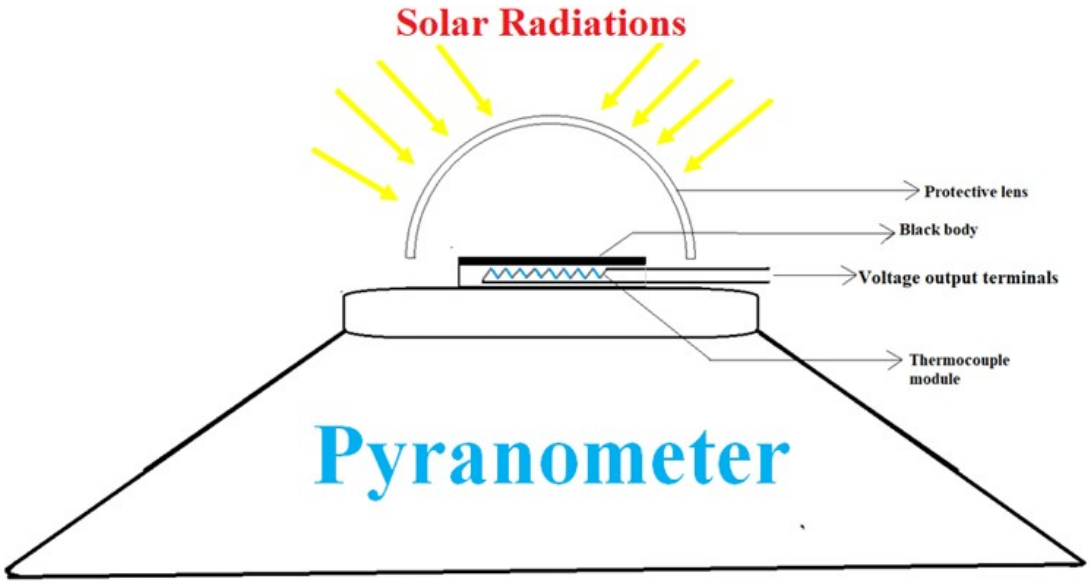

Figure 2.3. Pyranometer structure [44].

In contrast, a pyrheliometer is intended to measure direct normal irradiance, which is the power per unit area of a direct solar beam on a surface normal to the Sun.

Figure 2.4. Pyrheliometer [44].

A normal-incidence pyrheliometer is commonly installed atop a Sun-tracking device to keep it aimed at the Sun and exclude diffuse sky light [45].

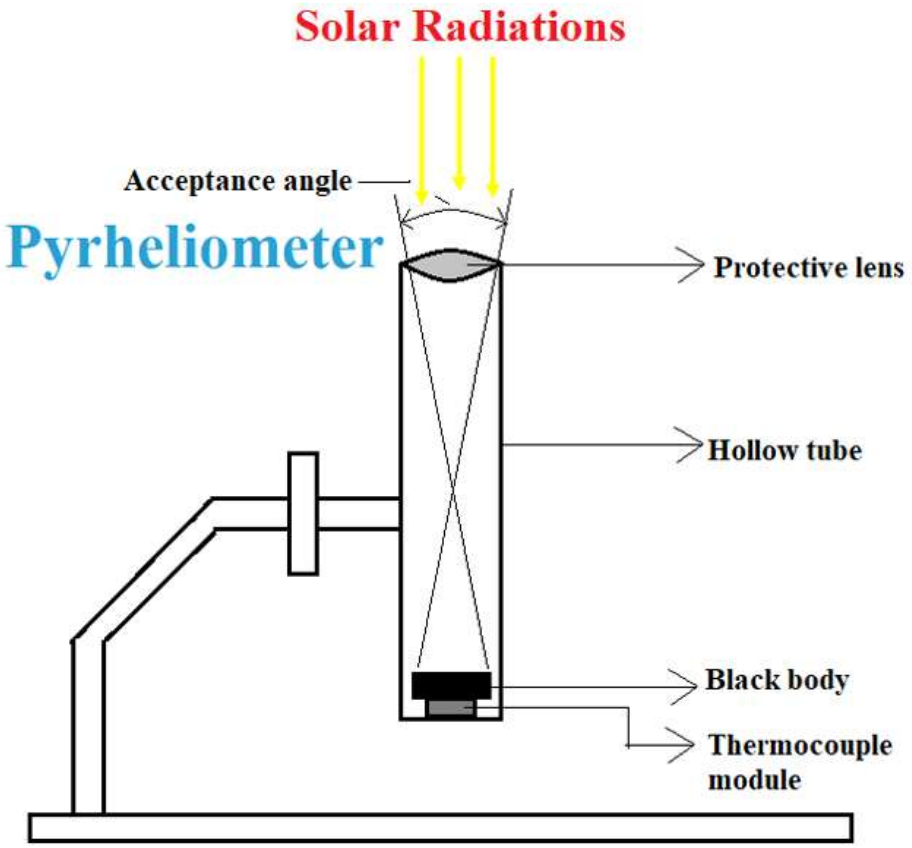

Figure 2.5. Pyrheliometer structure [44].

The global horizontal and direct normal measurements allow for the calculation of other quantities, such as diffuse horizontal irradiance by shading a pyranometer and plane-of-array irradiance on tilted collectors using global horizontal irradiance, diffuse irradiance, and solar geometry.

The spectroradiometer (or spectroradiometer) monitors spectral irradiance ($W/m^2/nm$) in UV, visible, and infrared bands. Spectroradiometers typically collect high-resolution spectral data using diffraction gratings and photodetector arrays. They are used in research and calibration to determine the detailed Sun spectrum, atmospheric absorption properties, and photosynthetically active radiation. In satellite remote sensing, spectrometers in orbit measure solar spectrum irradiance above the atmosphere, which is crucial for climate models. On the ground, spectral instruments (also known as Sun photometers or spectroradiometers) are used to estimate broadband values and atmospheric parameters.

Solar radiation is reported in two ways: similar but distinct. Irradiance is the power per unit area (W/m^2) from the Sun at a certain time or averaged over a short period. Pyranometers may directly measure this amount. Irradiation, also known as insolation,

refers to the total amount of solar energy received per unit area over time. It is typically measured in Wh/m² or kWh/m² per day or year. In other words, irradiance is an instantaneous flow, whereas irradiation is the same flux integrated over time. For instance, noon solar irradiance may be 900 W/m², while daily irradiation (energy) could be around 5-7 kWh/m². The standard meteorological units are W/m² for irradiance and kWh/m² or MJ/m² for accumulating energy.

In Turkey, ground observations have always been scarce. In the mid-2000s, an across the country project established twenty modern stations (equipped with pyranometers and pyrheliometers) around Turkey [46]. However, due to instrument and siting difficulties, only a handful of stations generated meaningful data during limited periods. According to B. Aksoy, just five stations produced reliable solar data for 2004-2005, making it impossible to map Turkey's solar climate based solely on ground data [46]. As a result, satellite datasets have been utilized to conduct national solar assessments. For instance, the NASA Surface Meteorology and Solar Energy (SSE) dataset (based on reanalysis and satellite inputs) was used to assess Turkey's solar resource [46]. NASA's Langley and Copernicus Atmosphere Monitoring Service (CAMS) provide similar satellite-based solar data for Europe.

3. TOTAL SOLAR RADIATION CALCULATIONS

The total quantity of solar energy that the Sun's rays reach a horizontal or inclined surface is referred to as total solar radiation.

Direct beam radiation, diffuse radiation, and ground-reflected radiation are its three primary constituents. Because it determines how much energy is available for solar panels to convert into heat or electricity, this parameter is essential in the field of solar energy and our thesis.

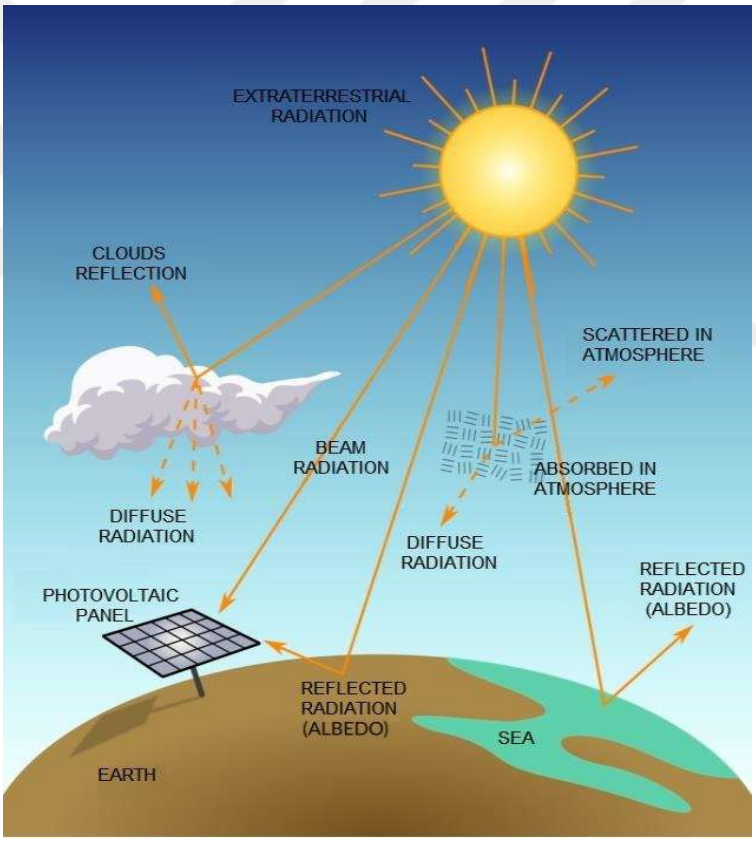

Figure 3.1. Solar radiation components [47].

Sunlight that has been scattered by dust, water vapor, molecules, and other atmospheric particles before it reaches the Earth's surface is known as diffuse radiation.

Beam radiation, also known as direct irradiance, is the amount of sunlight that goes in a straight line from the Sun to the surface without being scattered.

It has the highest energy density and is most effective when the solar panel is directly exposed to the Sun. Tracking systems are frequently employed to optimize the capture of this component throughout the day.

Reflected radiation, also known as albedo radiation, this radiation comes from the reflection of sunlight off the ground or surrounding surfaces.

The amount of reflected radiation depends on the ground surface properties. For example, snow-covered or sandy surfaces reflect more sunlight than vegetation or asphalt.

Even on cloudy or overcast days, diffuse radiation contributes significantly to the total solar energy received. While it is less intense than direct radiation, it is crucial for solar panel production, especially for locations with usual cloud cover.

The accuracy of solar calculations is dependent on the geographical location and latitude. The latitude angle for Sakarya, as previously mentioned, is 41.71°.

This latitude has an important role in setting solar angles and daylight length. All next calculations based on this exact location with same latitude angle.

3.1. Diffuse Solar Radiation Calculations

The best method to estimate the total solar radiation is to use specialized tools and sensors to take direct measurements. For every aspect of solar radiation, including diffuse radiation, these measurements offer reliable and accurate information. Unfortunately, measurement tools are not available. Therefore, a different approach has been used that is based on existing equations and models in which this study develops new diffuse solar radiation depends on pervious researches. These models offer a close approximation to actual conditions because they are based on observed or computed data. This study uses a comprehensive strategy by choosing 34 models from previous studies in order to improve reliability and accuracy. The variety of equations that estimate diffuse solar radiation under different circumstances. Give us a variety of results by computing diffused solar radiation using each model, capturing variances across various approaches and assumptions. This study calculates the average of these 34 results to further improve the estimation. Our presumed “measured value” for diffuse solar radiation in Sakarya city be this averaged value, which is measured value. To organize this, the 34 equation models are divided into five distinct

groups based on their characteristics, data requirements or mathematical structure. These groups help categorize the models, facilitating analysis, and enabling us to compare the performance and accuracy of different approaches.

The five groups are Diffuse fraction ($K_d = \frac{H_d}{H}$) calculated by clearness index ($K_t = \frac{H}{H_0}$), Diffuse fraction ($K_d = \frac{H_d}{H}$) calculated by sunshine fraction ($K_n = \frac{S}{S_0}$), Diffuse fraction ($K_d = \frac{H_d}{H}$) calculated by sunshine fraction ($K_n = \frac{S}{S_0}$) and clearness index ($K_t = \frac{H}{H_0}$), Diffuse coefficient ($K_{dd} = \frac{H_d}{H_0}$) calculated by clearness index ($K_t = \frac{H}{H_0}$), Diffuse coefficient ($K_{dd} = \frac{H_d}{H_0}$) calculated by sunshine fraction ($K_n = \frac{S}{S_0}$).

Where (H_d) is diffuse solar radiation, (H) is global solar radiation and (H_0) is extraterrestrial solar radiation. Also (S) are sunshine hours and (S_0) is maximum sunshine hours.

3.1.1. Maximum sunshine hours

Maximum sunshine hours (S_0), also called extraterrestrial day length, refers to the maximum possible duration of sunshine a location can receive in a day under clear sky conditions. It depends entirely on the geographical location (latitude (\phi)) and the day of the year (solar declination angle (δ)). This value is purely astronomical and does not consider actual weather or atmospheric conditions like clouds, pollution, or fog. It defines the upper limit of sunshine duration that can occur on a given day. S_0 is expressed in hours and ranges between 0 and 24.

The (S_0) is calculated by the following equation [35]:

$$S_0 = \frac{2}{15}\omega_s \tag{3.1}$$

Where sunrise hour angle (ω_s) calculated by the following equation [35]:

$$\omega_s = \cos^{-1}(-\tan\phi \tan\delta) \tag{3.2}$$

The solar declination angle (δ) is the angle between the Sun's rays and the Earth's equator. It varies throughout the year due to the tilt of the Earth's spinning axis (about 23.45°) and orbit around the Sun. This angle determines the Sun's position in the sky

at solar noon and has a significant impact on the amount of solar radiation received at any given location.

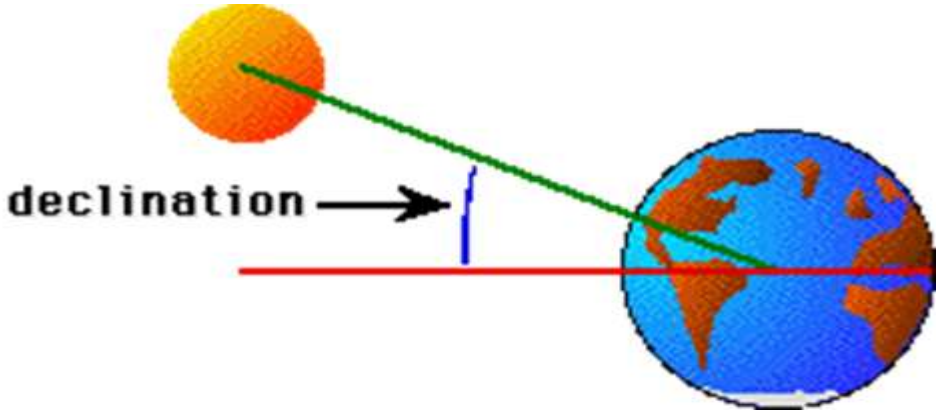

Figure 3.2. Solar declination angle.

The solar declination angle changes every day, ranging from +23.45° to -23.45° during the year. On the equinoxes, the declination is 0°, signifying that the Sun is directly above the equator.

Solar declination angle can be calculated by following equation [35]:

$$\delta = 23.45 \sin\left(\frac{360}{365}\left(284 + n_{day}\right)\right) \quad (3.3)$$

where n is the day of the year (January 1 = 1, February 1 = 32, March 1 = 60, etc..).

Table 3.1. Monthly average daily solar declination and sunrise hour angle.

Month	δ (°)	ω_s (°)	Month	δ (°)	ω_s (°)
January	-20.85	70.80	July	21.01	109.47
February	-13.33	78.17	August	13.30	101.81
March	-2.39	87.93	September	1.99	91.73
April	9.49	98.33	October	-9.85	81.35
May	18.81	107.12	November	-19.05	72.64
June	23.08	111.56	December	-23.01	68.42

The table shows the monthly average daily solar declination angles for the year. The angles range from -23.10 degrees in December to a maximum of 23.08 degrees in June. These angles represent the Sun's apparent movement north and south of the celestial equator over the course of a year. This information is critical for understanding the Sun's location and its effects on a variety of applications, including solar energy systems and architectural design. The previous table shows the monthly sunrise hour angles, which measure the Sun's angular distance from the east-west line at sunrise. The temperatures vary from 68.42 degrees in December to 111.56 degrees in June. Also, these angles are critical for estimating solar positions and determining daylight duration throughout the year.

Table 3.2. Maximum sunshine hours.

Month	S_0 (h)
January	9.44
February	10.42
March	11.72
April	13.11
May	14.28
June	14.88
July	14.60
August	13.57
September	12.23
October	10.85
November	9.68
December	9.12

The pervious table shows the maximum sunshine hours for each month of the year.

These numbers show the theoretical maximum amount of daylight accessible at a specific place on a clear day. The maximum value is in June with 14.88 hours, while the lowest is in December with 9.12 hours.

This variation reflects the changing length of the day caused by the Earth's axial tilt and orbit around the Sun. The data is critical for understanding seasonal variations in Sun availability. Maximum sunshine hours are affected by geographical location, particularly latitude.

3.1.2. Extraterrestrial solar radiation

Solar extraterrestrial radiation (H_0) is an incident of solar radiation on a surface at the top of the Earth's atmosphere. It shows the possibility of maximum solar energy obtainable before losses from air absorption, scattering, or reflection.

H_0 is an important reference in solar energy research as it is unaffected by weather or atmospheric conditions. It is used for calculating surface-level radiation, PV panel output, and thermal system performance.

Extraterrestrial radiation varies annually due to two astronomical factors: Earth-Sun distance and solar declination angle.

The average solar constant (G_{sc}) is around 1360.8 W/m² [35].

Extraterrestrial solar radiation estimates by following equation [23]:

$$H_0 = \frac{24}{\pi} G_{on} \left(\cos\phi \cos\delta \sin\omega_s + \frac{\pi}{180} \omega_s \sin\phi \sin\delta \right) \tag{3.4}$$

$$G_{on} = G_{sc} \left(1 + 0.033 \cos \frac{360 \cdot n_{day}}{365} \right) \tag{3.5}$$

On a given day (n_{day}), the instantaneous extraterrestrial (i.e. "just outside the atmosphere") solar irradiance on a surface normal (perpendicular) to the Sun's rays is known as "G_{on}." It is simply the solar constant G_{sc}, adjusted for the Earth's changing distance from the Sun during the year.

The data in the next table illustrate the seasonal variation in the availability of extraterrestrial solar radiation energy throughout the year. At the beginning of the year, solar irradiation is relatively low, indicating limited solar energy potential during the

winter months. As the months progress toward spring, the availability of solar radiation gradually increases, reflecting improved sunlight conditions and longer daylight hours. During spring, the solar energy potential becomes more favorable, and it continues to rise until it reaches its maximum in early summer. This period represents the peak of solar irradiance, with optimal conditions for solar energy generation due to stronger sunlight and clearer skies. Following the summer peak, the levels of extraterrestrial radiation begin to decline as the days become shorter and sunlight intensity decreases. This downward trend continues through the autumn months and into winter, when solar energy availability reaches its lowest point again.

Table 3.3. Monthly average daily extraterrestrial solar radiation on horizontal surface.

Month	H_0 (kWh/m²/day)
January	4.11
February	5.51
March	7.52
April	9.56
May	11.01
June	11.60
July	11.28
August	10.08
September	8.20
October	6.09
November	4.41
December	3.68

The data in the previous table show how the availability of extraterrestrial solar radiation energy varies by month.

January's value of 4.11 kWh/m²/day shows low solar irradiation at the start of the year. H_0 levels steadily rise over time, peaking at 7.52 kWh/m²/day in March and 5.51 kWh/m²/day in February, respectively. By April, the number increases to 9.56 kWh/m²/day, showing great solar energy potential. Solar irradiance peaks in June at 11.60 kWh/m²/day, then decreases slightly in July to 11.28 kWh/m²/day during the winter. The values continued decreasing in the second half of the year, dropping to 8.20 kWh/m²/day in September and gradually decreasing to 3.68 kWh/m²/day in December. This pattern emphasizes the seasonal nature of solar energy availability, with the highest values occurring during the summer months and the lowest during winter.

3.1.3. Diffuse solar radiation models

The five groups are Diffuse fraction ($K_d = \frac{H_d}{H}$) calculated by clearness index ($K_t = \frac{H}{H_0}$), Diffuse fraction ($K_d = \frac{H_d}{H}$) calculated by sunshine fraction ($K_n = \frac{S}{S_0}$), Diffuse fraction ($K_d = \frac{H_d}{H}$) calculated by sunshine fraction ($K_n = \frac{S}{S_0}$) and clearness index ($K_t = \frac{H}{H_0}$), Diffuse coefficient ($K_{dd} = \frac{H_d}{H_0}$) calculated by clearness index ($K_t = \frac{H}{H_0}$), Diffuse coefficient ($K_{dd} = \frac{H_d}{H_0}$) calculated by sunshine fraction ($K_n = \frac{S}{S_0}$).

Where (H_d) is diffuse solar radiation, (H) is global solar radiation and (H_0) is extraterrestrial solar radiation. Also (S) is sunshine hours and (S_0) is maximum sunshine hours.

The (H_0) and (S_0) and other components have been calculated. also, there are components like (H) and (S), The values of (H) and (S) can be found from Güneş Enerjisi Potansiyel Atlası (GEPA) [48], which is ais a powerful solar energy mapping tool created by the Turkish Ministry of Energy and Natural Resources. It gives thorough information on Sun irradiation levels in various parts of Turkey throughout the year.

Table 3.4. Global solar Radiation for Sakarya.

Month	H (kWh/m²/day)
January	1.42
February	2.29
March	3.28
April	4.41
May	5.64
June	6.01
July	5.84
August	5.27
September	4.19
October	2.86
November	1.69
December	1.23

The last table shows a critical parameter in our calculations, which is global solar radiation for Sakarya. It shows the seasonal variations in solar energy availability throughout the year. January records the lowest value at 1.42 kWh/m²/day, indicating limited solar potential during the winter months. As the year progresses, solar radiation increases, reaching 2.29 in February and 3.28 in March. By April and May, the values rise significantly to 4.41 and 5.64 kWh/m²/day, respectively, showing improved conditions for solar energy utilization. The highest solar radiation is observed in June with a value of 6.01 kWh/m²/day, followed by a slight decline in July to 5.846.01 kWh/m²/day. During the late summer and autumn months, solar radiation continues to decrease gradually, falling to 4.19 kWh/m²/day in September and further down to 2.86kWh/m²/day in October. This decreasing pattern continues into the final months

of the year, ending with 1.69 kWh/m²/day in November and 1.23 kWh/m²/day in December.

Table 3.5. Sunshine hours in Sakarya.

Month	S (h)
January	3.20
February	4.23
March	5.01
April	6.33
May	8.39
June	9.72
July	10.35
August	9.56
September	8.01
October	5.53
November	4.05
December	3.09

The data show an interesting seasonal variation, with the lowest figure recorded in December at 3.09 hours per day. Sunshine hours rise progressively from winter to spring, from 3.20 hours in January to 5.01 hours in March. By April, the daily sunshine length had reached 6.33 hours, and it continues to grow strongly through May and June, peaking at 9.72 hours in June. July has the most daily sunshine of 10.35 hours, showing that this month is ideal for solar energy. A small reduction is observed in August, with 9.56 hours of sunshine, followed by an ongoing decrease throughout the autumn. September has 8.01 hours of sunlight per day, which decreases to 5.53 hours in October and 4.05 hours in November.

3.1.3.1. Diffuse fraction calculated by clearness index

The $K_d = \frac{H_d}{H}$ and $K_t = \frac{H}{H_0}$

Model equation 1 [15]:

$$K_d = 1.0896 - 1.4797K_t + 0.1471{K_t}^2 \quad (3.6)$$

Model equation 2 [15]:

$$K_d = 13.9375 - 76.276K_t + 144.3846{K_t}^2 - 92.148{K_t}^3 \quad (3.7)$$

Model equation 3 [15]:

$$K_d = 1.0492 - 1.3246K_t \quad (3.8)$$

Model equation 4 [17]:

$$K_d = 1.0212 - 1.1672K_t \quad (3.9)$$

Model equation 5 [17]:

$$K_d = 1.1244 - 1.5582K_t + 0.3635{K_t}^2 \quad (3.10)$$

Model equation 6 [17]:

$$K_d = 1.711 - 4.9062K_t + 6.6711{K_t}^2 - 3.9235{K_t}^3 \quad (3.11)$$

Model equation 7 [20]:

$$K_d = 0.9885 - 1.4276K_t + 0.5679{K_t}^2 \quad (3.12)$$

Model equation 8 [20]:

$$K_d = 1.027 - 1.6582K_t + 1.1018{K_t}^2 - 0.4019{K_t}^3 \quad (3.13)$$

Model equation 9 [18]:

$$K_d = 1.039 - 1.741{K_t}^2 \quad (3.14)$$

Model equation 10 [18]:

$$K_d = -5.759 + 35.093K_t - 61.052{K_t}^2 + 33.115{K_t}^3 \quad (3.15)$$

Model equation 11[49]:

$$K_d = 1.00 - 1.13K_t \quad (3.16)$$

Model equation 12 [16]:

$$K_d = 0.789 - 0.869K_t \quad (3.17)$$

Model equation 13 [19]:

$$K_d = -0.193 + 0.343\frac{1}{K_t} \quad (3.18)$$

Model equation 14 [21]:

$$K_d = 1.39 - 4.027K_T + 5.531{K_t}^2 - 3.108{K_t}^3 \quad (3.19)$$

Model equation 15 [22]:

$$K_d = 1.317 - 3.023K_t + 3.372{K_t}^2 - 1.769{K_t}^3 \quad (3.20)$$

Model equation 16 [14]:

$$K_d = 1.6932 - 8.2262K_t + 25.5532{K_t}^2 - 37.807{K_t}^3 + 19.8178{K_t}^4 \quad (3.21)$$

Model equation 17 [26]:

$$K_d = 0.583 + 0.9985K_t - 5.24{K_t}^2 + 5.322{K_t}^3 \quad (3.22)$$

3.1.3.2. Diffuse fraction calculated by sunshine fraction

Model equation 18 [15]:

$$K_d = 0.6603 - 0.5272K_n \quad (3.23)$$

Model equation 19 [15]:

$$K_d = 0.7434 - 0.8203K_n + 0.2454(K_n)^2 \quad (3.24)$$

Model equation 20 [17]:

$$K_d = 0.663 - 0.4883K_n \quad (3.25)$$

Model equation 21 [17]:

$$K_d = 0.6492 - 0.4323K_n - 0.0512(K_n)^2 \quad (3.26)$$

Model equation 22 [17]:

$$K_d = 0.5562 + 0.1536K_n - 1.2027(K_n)^2 + 0.7122(K_n)^3 \quad (3.27)$$

3.1.3.3. Diffuse fraction calculated by clearness index and sunshine fraction

Model equation 23 [50]:

$$K_d = 1.194 - 0.838K_t - 0.446K_n \quad (3.28)$$

Model equation 24 [51]:

$$K_d = 0.9593 - 0.8713K_t + 0.29191{K_t}^2 - 0.0979{K_t}^3 - 0.28419(K_n) + 0.0253(K_n)^2 - 0.02083(K_n)^3 \quad (3.29)$$

3.1.3.4. Diffuse coefficient calculated by clearness index

Where $K_{dd} = \frac{H_d}{H_o}$

Model equation 25 [17]:

$$K_{dd} = 0.331 - 0.233K_t \quad (3.30)$$

Model equation 26 [17]:

$$K_{dd} = 0.0511 + 0.8267{K_t}^2 - 0.9854{K_t}^3 \quad (3.32)$$

Model equation 27 [17]:

$$K_{dd} = 0.3276 - 0.7515K_t + 1.9883{K_t}^2 - 1.8497{K_t}^3 \quad (3.32)$$

Where $K_{dd} = \frac{H_d}{H_o}$

3.1.3.5. Diffuse coefficient calculated by sunshine fraction

Model 29 [17]:

$$K_{dd} = 0.2593 - 0.0978K_n \quad (3.33)$$

Model 30 [17]:

$$K_{dd} = 0.2142 + 0.0863K_n - 0.1684(K_n)^2 \quad (3.34)$$

Model 31 [17]:

$$K_{dd} = 0.2427 - 0.0933K_n + 0.1846(K_n)^2 - 0.2184(K_n)^3 \quad (3.35)$$

Model 32 [15]:

$$K_{dd} = 0.2626 - 0.1391K_n \quad (3.36)$$

Model 33 [15]:

$$K_{dd} = 0.2205 - 0.0126K_n - 0.1292(K_n)^2 \quad (3.37)$$

Model 34 [19]:

$$K_{dd} = 0.293 - 0.135K_n \quad (3.38)$$

3.1.4. Develop new model of diffuse solar radiation

As I mentioned before, this study calculates the average of these 34 results to further improve the estimation, and the averaged value used as the "measured value" for diffuse solar radiation in Sakarya city. Based on this "measured value" the new diffuse solar radiation model has been developed.

Table 3.6. Average of 34 diffuse solar radiation model 'measured value'.

Month	H_d(kWh/m²/day)
January	0.87
February	1.19
March	1.64
April	2.07
May	2.31
June	2.38
July	2.26
August	2.03
September	1.68
October	1.31
November	0.94
December	0.77

From the previous table, a new model can be developed; this model is based on multiple linear regression. A statistical technique that creates a linear relationship between a dependent variable (in this case, diffuse radiation, or (H_d)) and several independent variables (K_t), $((K_t)^2)$, (K_n), $((K_n)^2)$.

Where (C_0), (C_1), (C_2), (C_3), (C_4), are regression coefficients.

$$K_d = C_0 + C_1K_t + C_2(K_t)^2 + C_3(K_n) + C_4(K_n)^2 \quad (3.39)$$

I used polynomial function to cover all points and make close result as much as (H_d) measured values.

New diffuse solar radiation equation model for Sakarya:

$$Kd = 1.2625 - 2.1773K_t + 1.4192(K_t)^2 - 0.2060K_n + 0.0388(K_n)^2 \quad (3.40)$$

This model which is made by linear regression method by using MATLAB should give diffuse solar radiation values as close as measured diffuse solar radiation values from pervious table.

The measured value and new model equation value is statistically tested using a variety of test methods, as follows:

Relative percentage error (E):

$$E = \frac{c_i - m_i}{m_i} \cdot 100 \quad (3.41)$$

Coefficient of determination (R^2):

$$R^2 = \frac{\sum_{i=1}^{n}(c_i - \bar{c})(m_i - \bar{m})}{\sqrt{\sum_{i=1}^{n}(c_i - \bar{c})^2} \cdot \sqrt{\sum_{i=1}^{n}(m_i - \bar{m})^2}} \quad (3.42)$$

Mean percentage error (MPE):

$$MPE = \frac{\sum_{i=1}^{n} E}{n} \quad (3.43)$$

Mean absolute percentage error (MAPE):

$$MAPE = ABS\left(\frac{\sum_{i=1}^{n} E}{n}\right) \quad (3.44)$$

Relative standard error (RSE):

$$RSE = \sqrt{\frac{SSRE}{n}} \quad (3.45)$$

Sum of the squares of relative errors (SSRE):

$$SSRE = \sum_{i=1}^{n} \left(\frac{c_i - m_i}{m_i}\right)^2 \quad (3.46)$$

Mean bias error (MBE):

$$MBE = \frac{1}{n}\sum_{i=1}^{n}(c_i - m_i) \quad (3.47)$$

Root mean square error (RMSE):

$$RMSE = \sqrt{\frac{1}{n}\sum_{i=1}^{n}(c_i - m_i)^2} \quad (3.48)$$

Where (c) and (m) are calculated and measured value respectively.

Table 3.7. Results of statistical test methods.

Statistical methods	Values
MPE (%)	0.0001%
SSRE	0.0000
RSE	0.0011
RMSE (kWh/m²)	0.0018
MBE ((kWh/m²)	0.0001
R^2	1.0000

The pervious table shown an extremely high level of accuracy, with errors approaching zero and an R^2 value of 1.0000.

A near-perfect fit is observed between the new model's solar radiation values and measured values.

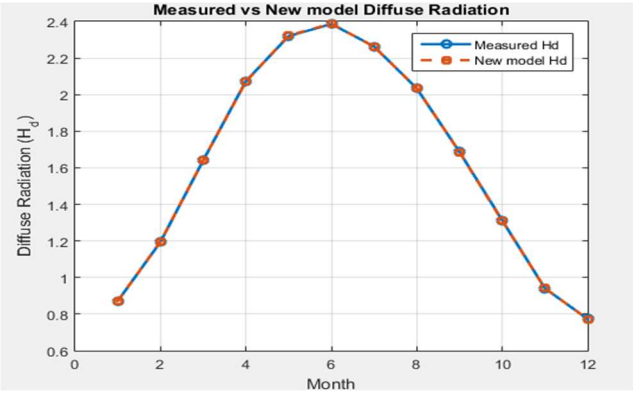

Figure 3.3. Measured values VS new model solar radiation values.

Table 3.8. Monthly average daily new diffuse solar radiation model values.

Month	H_d(kWh/m²/day)
January	0.87
February	1.20
March	1.64
April	2.07
May	2.32
June	2.39
July	2.26
August	2.03
September	1.69
October	1.31
November	0.94
December	0.79

The pervious table represent monthly average daily new model of diffuse solar radiation. The seasonal variation can be observed, with the lowest value in December

(0.79 kWh/m²/day) and the highest in June (2.39 kWh/m²/day). Diffuse radiation gradually increases from winter to early summer, peaking during the sunniest months when atmospheric scattering is greatest.

3.2. Beam Radiation Calculations

By using diffuse solar radiation results, the next step is calculating beam solar radiation by using the following equation:

$$H_b = H - H_d \tag{3.49}$$

Where H_b is the beam solar radiation and H_d is a new model of diffuse solar radiation.

Table 3.9. Monthly average daily beam solar radiation values.

Month	H_b(kWh/m²/day)
January	0.55
February	1.09
March	1.64
April	2.34
May	3.32
June	3.62
July	3.58
August	3.24
September	2.50
October	1.55
November	0.75
December	0.51

The data shows a strong seasonal variation, with the lowest value in December (0.51 kWh/m²/day) and the highest in June (3.62 kWh/m²/day). It rises from winter to spring, peaking in the early summer months when the Sun's intensity is at its highest. Solar radiation components consistently peak in June and reach their lowest values in December.

3.3. Maximum Total Solar Radiation Calculated for Inclined Surface

This section demonstrates the significant role of inclination angle in determining total solar radiation received. There is a specific tilt angle at which solar panels should be mounted to capture and collect the maximum possible total solar radiation. This approach significantly increases the power generation potential of photovoltaic panels. The maximum total solar radiation with respect to the tilt angle is calculated using the following equation:

$$H_t = H_b R_b + H_d R_d + H(\rho_g)\frac{1-\cos\beta}{2} \tag{3.50}$$

Where (β) is the tilt angle of the surface or PV panels and (ρ_g) is the ground reflectivity coefficient, and its value is (0.2).

R_b is the tilt coefficient of beam radiation can be calculated through the following equation:

$$R_b = \frac{\cos(\phi-\beta)\cos(\delta)\sin(\omega_s^{'}) + \left(\frac{\pi}{180}\right)\omega_s^{'}\sin(\phi-\beta)\sin(\delta)}{\cos(\phi)\cos(\delta)\sin(\omega_s) + \left(\frac{\pi}{180}\right)\omega_s\sin(\phi)\sin(\delta)} \tag{3.51}$$

R_d is the tilt coefficient of diffuse solar radiation can be calculated through the following equation:

$$R_d = \frac{1+\cos\beta}{2} \tag{3.52}$$

$\omega_s^{'}$ is the sunrise hour angle for tilted surface can be calculated through the next equation:

$$\omega_s^{'} = \min(\cos^{-1}(-\tan(\phi)\cdot\tan(\delta)), \cos^{-1}(-\tan(\phi-\beta)\cdot\tan(\delta))) \tag{3.53}$$

By using MATLAB, the tilt angle has been calculated through changing the tilt angle from 0 degrees to 90 degrees by one step angle, the angle with highest total solar radiation is the optimum tilt angle.

Table 3.10. Monthly average daily maximum total solar radiation values and optimum tilt angles.

Month	H_t(kWh/m²/day)	Optimum tilt angle (°)
January	2.15	57.16
February	3.20	51.04
March	3.86	36.94
April	4.63	20.83
May	5.68	7.26
June	6.01	0.10
July	5.85	3.19
August	5.44	16.65
September	4.81	33.47
October	3.91	48.65
November	2.61	57.20
December	2.10	60.42

Where the yearly average daily optimum tilt angle is (32.64°).

3.4. Maximum Total Solar Radiation for East and West Orientations

In this part, the maximum total solar radiation has been calculated in inclined surface for East and West orientations.

The same equation for total solar radiation is used, with a new parameters and change some exist parameters as follows [32]:

$$\begin{aligned} R_b = & \left[\cos\beta \sin\delta \sin\phi \frac{\pi}{180}(\omega_{ss} - \omega_{sr}) - \right. \\ & \sin\delta \cos\phi \sin\beta \cos\gamma \frac{\pi}{180}(\omega_{ss} - \omega_{sr}) + \\ & \cos\delta \cos\delta \sin s \cos\beta (\sin\omega_{ss} - \sin\omega_{sr}) + \\ & \cos\delta \cos\gamma \sin\phi \sin s (\sin\omega_s - \sin\omega_{sr}) - \\ & \left.\cos\delta \sin\beta \sin\gamma (\cos\omega_{ss} - \cos\omega_{sr})\right] / 2 \left[\cos\phi \cos\delta \sin\omega_s + \right. \\ & \left.\frac{\pi}{180}\omega_s \sin\phi \sin\delta\right] \end{aligned} \tag{3.54}$$

Where γ is the surface azimuth angle. In east γ is -90° and west is 90°, also ω_{ss} is sunset hour angle and ω_{sr} is sunrise hour angle.

If γ is 90° (west-facing panels) [32]:

$$\omega_{sr} = -\min\left[\omega_s, \cos^{-1}\left(\frac{AB - \sqrt{A^2 - B^2 + 1}}{A^2 + 1}\right)\right] \tag{3.55}$$

$$\omega_{ss} = \min\left[\omega_s, \cos^{-1}\left(\frac{AB + \sqrt{A^2 - B^2 + 1}}{A^2 + 1}\right)\right] \tag{3.56}$$

If γ is -90° (east-facing panels):

$$\omega_{sr} = -\min\left[\omega_s, \cos^{-1}\left(\frac{AB + \sqrt{A^2 - B^2 + 1}}{A^2 + 1}\right)\right] \tag{3.57}$$

$$\omega_{ss} = \min\left[\omega_s, \cos^{-1}\left(\frac{AB - \sqrt{A^2 - B^2 + 1}}{A^2 + 1}\right)\right] \tag{3.58}$$

A and B can be expressed by the following equation [32]:

$$A = \frac{\cos\phi}{(\sin\gamma \tan\beta)} + \frac{\sin\phi}{\tan\gamma} \tag{3.59}$$

$$B = \tan\delta\left(\frac{\cos\phi}{\tan\gamma} - \frac{\sin\phi}{\sin\gamma \tan\beta}\right) \tag{3.60}$$

The optimum tilt angle was determined using MATLAB by varying the tilt angle from 0° to 90° in 1-degree instep. The tilt angle that provided the maximum total solar

radiation was selected as the optimum and the results showed that for azimuth angles of $\gamma = 90°$ (west-facing) and $\gamma = -90°$ (east-facing), the optimum tilt angle is 0°, meaning that panels mounted horizontally receive more solar radiation than those tilted toward the east or west. However, some roofs may not allow horizontal mounted system. Therefore, in the simulation chapter using PV*SOL, alternative tilt angles suitable for east and west orientations will be explored to provide practical installation solutions.

4. SIMULATIONS AND SOILING IMPACTS

This section presents simulations of the PV roof system, which has been built on the roof of the Electrical and Electronics Engineering faculty at Sakarya University. Our aim from this simulation is to understand the effect of inclination angle and orientation in generating electricity, and what is the optimum tilt angle and orientation for the software.

The PV roof simulation incorporates SPE 400 mono-crystalline modules from SCHMID\PEKENTAŞ with 400-Watt peak power, 41.46 Volt maximum power voltage, 9.66 Amper, and its efficiency is 20.10%. There are three panels with 32° inclination angles mounted for each direction, east, west, south, and three horizontally. The system involves a MIC 1000TL-X inverter (1000 VA apparent power, 4.8 A max output current).

Figure 4.1. PV rooftop system at M6 building.

The last figure shows our PV rooftop system that built on the roof Electrical and Electronic engineering building. There are three panels with 32° tilt angles facing East, West and South orientations with three panels horizontally.

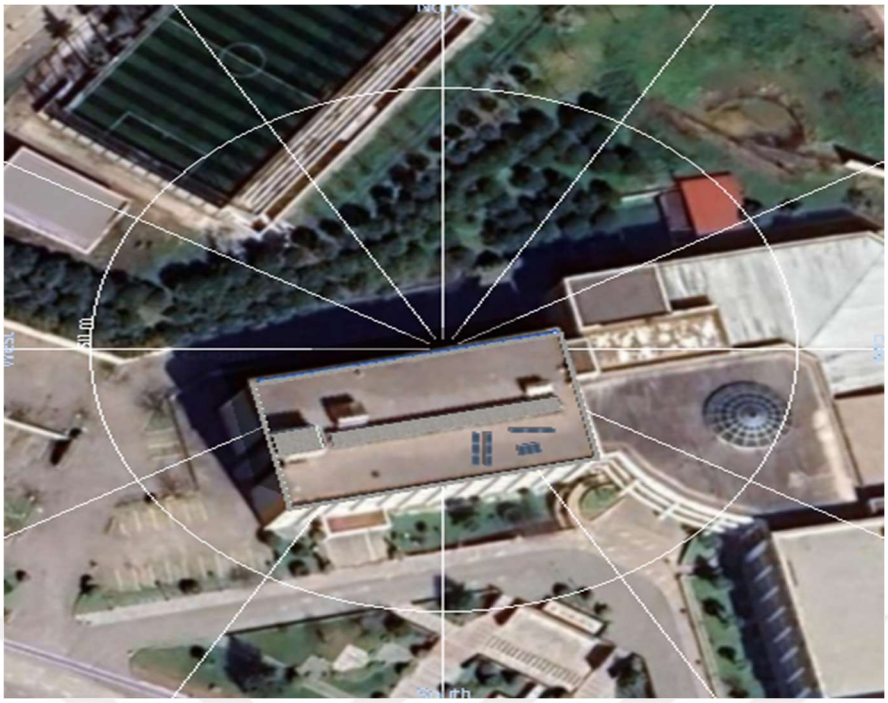

Figure 4.2. PV rooftop system at M6 building by using PV*SOL.

The previous figure is a 3D model of a PV rooftop system on Electric and Electronics Engineering faculty at Sakarya University.

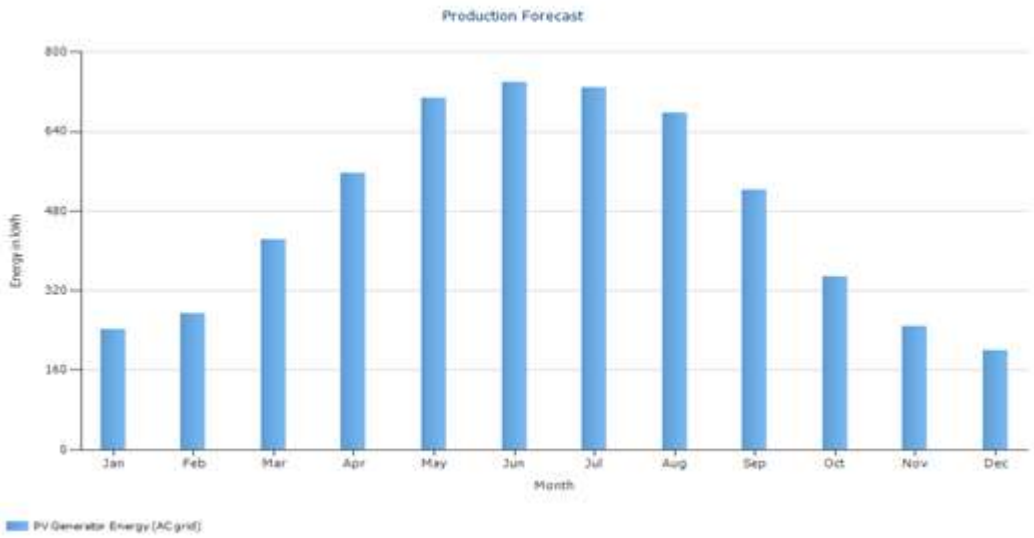

Figure 4.3. Production forecast from the software for the PV roof system.

According to the PVSOL software, the PV system exports energy to the grid with the value of 5660 kWh/Year.

east		
PV Generator Output	1.20	kWp
PV Generator Surface	5.97	m²
Global Radiation at the Module	1328.45	kWh/m²
Global Radiation on Module without reflection	1394.14	kWh/m²
Performance Ratio (PR)	81.90	%
PV Generator Energy (AC grid)	1371.92	kWh/Year
Spec. Annual Yield	1143.27	kWh/kWp
zero		
PV Generator Output	1.20	kWp
PV Generator Surface	5.97	m²
Global Radiation at the Module	1377.55	kWh/m²
Global Radiation on Module without reflection	1448.62	kWh/m²
Performance Ratio (PR)	81.66	%
PV Generator Energy (AC grid)	1421.22	kWh/Year
Spec. Annual Yield	1184.35	kWh/kWp
south		
PV Generator Output	1.20	kWp
PV Generator Surface	5.97	m²
Global Radiation at the Module	1583.58	kWh/m²
Global Radiation on Module without reflection	1645.69	kWh/m²
Performance Ratio (PR)	82.56	%
PV Generator Energy (AC grid)	1632.53	kWh/Year
Spec. Annual Yield	1360.44	kWh/kWp

Figure 4.4. Software simulation result per model area.

west		
PV Generator Output	1.20	kWp
PV Generator Surface	5.97	m²
Global Radiation at the Module	1211.98	kWh/m²
Global Radiation on Module without reflection	1286.23	kWh/m²
Performance Ratio (PR)	79.89	%
PV Generator Energy (AC grid)	1234.60	kWh/Year
Spec. Annual Yield	1028.83	kWh/kWp

Figure 4.5. Software simulation result per model area for west-facing panels.

Comparison of four PV system orientations (west, east, zero (horizontal), and south), shows that the south-facing orientation exceeds all others in power output. It has the highest global radiation on the module (1645.69 kWh/m²), the highest performance ratio (82.56%), and the highest annual energy output (1632.53 kWh/year), leading to the highest specific annual yield (1360.44 kWh/kWp). The zero (horizontal) orientation yields (1421.22 kWh/year) and (1184.35 kWh/kWp), thanks to balanced exposure throughout the day. The east orientation produces somewhat less than the flat layout, yielding (1371.92 kWh/year) with a specific yield of (1143.27 kWh/kWp) and a performance ratio of (81.90%). Lastly, the west-facing setup shows the lowest performance, with only 1234.60 kWh/year and a specific yield of 1028.83 kWh/kWp, and the lowest PR at (79.89%).

east			
Global radiation - horizontal	**1,478.31**	**kWh/m²**	
Deviation from standard spectrum	-14.78	kWh/m²	-1.00 %
Ground Reflection (Albedo)	22.24	kWh/m²	1.52 %
Orientation and inclination of the module surface	-91.63	kWh/m²	-6.17 %
Module-independent shading	0.00	kWh/m²	0.00 %
Reflection on the Module Surface	-65.69	kWh/m²	-4.71 %
Global Radiation at the Module	**1,328.45**	**kWh/m²**	
zero			
Global radiation - horizontal	**1,478.31**	**kWh/m²**	
Deviation from standard spectrum	-14.78	kWh/m²	-1.00 %
Ground Reflection (Albedo)	0.00	kWh/m²	0.00 %
Orientation and inclination of the module surface	-0.01	kWh/m²	0.00 %
Module-independent shading	-14.90	kWh/m²	-1.02 %
Reflection on the Module Surface	-71.07	kWh/m²	-4.91 %
Global Radiation at the Module	**1,377.55**	**kWh/m²**	
south			
Global radiation - horizontal	**1,478.31**	**kWh/m²**	
Deviation from standard spectrum	-14.78	kWh/m²	-1.00 %
Ground Reflection (Albedo)	22.24	kWh/m²	1.52 %
Orientation and inclination of the module surface	159.92	kWh/m²	10.76 %
Module-independent shading	0.00	kWh/m²	0.00 %
Reflection on the Module Surface	-62.11	kWh/m²	-3.77 %
Global Radiation at the Module	**1,583.58**	**kWh/m²**	

Figure 4.6. Software simulation result irradiance analysis.

west			
Global radiation - horizontal	**1,478.31**	**kWh/m²**	
Deviation from standard spectrum	-14.78	kWh/m²	-1.00 %
Ground Reflection (Albedo)	22.24	kWh/m²	1.52 %
Orientation and inclination of the module surface	-192.13	kWh/m²	-12.93 %
Module-independent shading	-7.41	kWh/m²	-0.57 %
Reflection on the Module Surface	-74.25	kWh/m²	-5.77 %
Global Radiation at the Module	**1,211.98**	**kWh/m²**	

Figure 4.7. Software simulation irradiance analysis results for west-facing panels.

The last two figures show how the same horizontal irradiation of 1478.31 kWh/m² is redistributed while tilting and facing the PV modules in different orientations. In the case of (horizontal modules). It is collecting 1377.55 kWh/m² on its surface, losing roughly 1% ($-14.78\ \mathrm{kWh/m^2}$) due to spectrum deviation, another 1.02% ($-14.90\ \mathrm{kWh/m^2}$) due to module-independent shading, and a further 4.91% ($-71.07\ \mathrm{kWh/m^2}$) from module reflection. The tilt of east-facing modules reduces direct incidence by -6.17% (-91.63 kWh/m²) and another -4.71% (-65.69 kWh/m²) from the module reflection, while south-facing modules perform best at 1,583.58 kWh/m², gaining +10.76% (159.92 kWh/m²) from optimal tilt and orientation even after a -3.77% ($-62.11\ \mathrm{kWh/m^2}$) 62.11 kWh/m²) reflection loss. In the second figure,

west-facing modules fare worst at 1,211.98 kWh/m², the –12.93 % (–192.13 kWh/m²) due to the orientation, also there is a loss by –5.77% (–74.25 kWh/m²) due to reflection.

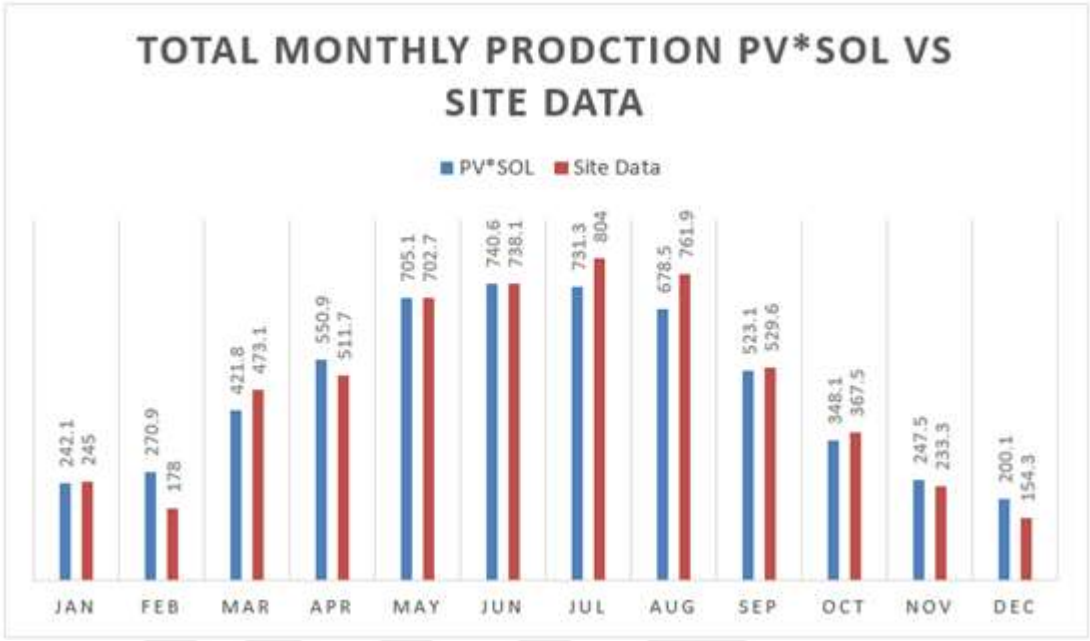

Figure 4.8. Total monthly production PV*SOL vs site data.

The chart presents a detailed comparison between the monthly solar energy production values obtained from PVSOL simulation software and the actual measured data collected from the site, both expressed in kilowatt-hours (kWh). Overall, the data sets demonstrate a consistent trend throughout the year, with both the simulated and actual values generally rising and falling in a similar pattern that reflects seasonal solar radiation variations. This alignment suggests that PVSOL is capable of accurately estimating solar energy output under typical weather and operational conditions. However, some discrepancies are observed in specific months due to external environmental factors or unexpected weather events. As expected, the peak solar energy production is recorded during the summer months—June, July, and August—owing to longer days and more intense solar irradiance. These months exhibit higher alignment between simulated and measured outputs, further affirming the software's reliability during optimal solar conditions. Despite the few monthly deviations, the overall annual error across all months is just 0.68%, indicating a strong correlation between the simulated projections and the real-world performance. This demonstrates that PV*SOL can be a reliable and useful tool for forecasting solar energy production, especially when supplemented with site-specific environmental inputs for enhanced accuracy.

Table 4.1. Total energy production from PV*SOL simulation and site data.

Month	PV*SOL (KWh)	Site Data (KWh)	Error %
January	242.1	245	1.18
February	270.9	178	52.13
March	421.8	473.1	10.84
April	550.9	511.7	7.66
May	705.1	702.7	0.34
June	740.6	738.1	0.34
July	731.3	804	9.04
August	678.5	761.9	10.96
September	523.1	529.6	1.23
October	348.1	367.5	5.29
November	247.5	233.3	6.10
December	200.1	154.3	29.94
Total	5660	5699.2	0.68

In details the chart shows a comparison between the monthly solar energy production from PV*SOL software and the actual measured data from the site, in kilowatt-hours (kWh). In general, the two sets of data follow a similar pattern across the year, but there are some differences. The smallest errors are in May and June, both with about 0.34% errors, showing very close results. Some months have larger differences, such as February with a 52.13% that's due to heavy snow falling during this month and December with 29.94% error. The highest solar energy production happens in the summer months like June, July, and August, which is expected because of stronger sunlight. Overall, PV*SOL simulations give a good result with 0.68% total error.

PV*SOL also was used to determine the optimum tilt angle for east and west-oriented panels by adjusting the tilt from 0° to 90°. The angle that provides the highest energy production is considered the optimum tilt angle. For east-facing panels, the optimum tilt angle was found to be between 8° and 9°.

The next four figures present different scenarios where PV*SOL was used to design a fully covered PV solar system roof for each direction: south, east, west, and horizontal, in order to determine the most efficient solution.

Number of Covered Areas	1
Number of PV Modules	60
Number of Inverters	10
PV Generator Output	24 kWp

Figure 4.9. Completely covered roof with solar panels facing west.

Number of Covered Areas	1
Number of PV Modules	60
Number of Inverters	10
PV Generator Output	24 kWp

Figure 4.10. Completely covered roof with horizontal solar panels.

Number of Covered Areas	1
Number of PV Modules	59
Number of Inverters	7
PV Generator Output	23.6 kWp

Figure 4.11. Compeletely covered roof with solar panels facing south.

Number of Covered Areas	1
Number of PV Modules	63
Number of Inverters	7
PV Generator Output	25.2 kWp

Figure 4.12. Completely covered roof with solar panels facing east.

The last four figures show different solutions for our roof and indicate whether we can fully cover it with solar panels. For the panels facing west, 60 panels could be installed; for panels facing the east, 63 panels; for the horizontal panels, 60 panels; and for the panels facing south, 59 panels. Although the south side has the fewest panels, it produces the highest energy at 31,101 kWh per year. The horizontal comes second with 28,560 kWh per year, followed by the east side with 27,722 kWh per year, and the west side with the lowest production at 23,676 kWh per year. The system budget

is an important factor. Installing tilted panels like those on the south side generally costs more due to additional equipment and extra effort during installation, even though fewer panels are needed. On the other hand, horizontal panels are cheaper and easier to install but require more maintenance and higher cleaning costs over time to maintain good efficiency. So, the south facing panels offer the best energy production but come with higher installation costs, while horizontal panels provide a less installation cost but require more in cleaning and maintaining in a long term.

4.1. Soiling Impact

The soiling factor represents the reduction in incident solar radiation on PV panels caused by dust, dirt, and other deposits on the module surface, which effectively quantifies the loss of power output. In other words, soiling blocks or scatters sunlight (also known as hard or soft shading), reducing PV efficiency [52].

Even small soiling losses might be significant: Without cleaning, soiling reduced PV energy yield by 3-4% [52]. Meteorological modelling suggests that extremely dirty or arid-like deserts may lose over 50% of their generation capacity [53].

Wetter or less dusty areas have significantly located in northern and central Europe have significantly lower soiling losses, on the order of 0-1% per year if rainfall washes the panels on a regular basis, while drier Mediterranean or Southern European sites see higher seasonal losses. A recent pan-European study indicated that average annual soiling loss is only 0.9% if rain fully cleans the panels, rising to nearly 5.3% with less effective rainfall [54].

An experiment in Istanbul indicated that uncleaned panels lost approximately 0.4% of their power after 3 days, but up to 3.0% after 24 days without rain, indicating moderate soiling rates in a coastal city area. Even small percentage losses can have a significant impact on performance [55].

To reduce the soiling effects, PV operators use both preventive and corrective techniques. Preventive strategies include locating arrays away from dust sources, including deserts, dry agricultural lands, and industrial emissions, optimizing module tilt and arrangement, and adopting self-cleaning surface coatings. Corrective actions often entail regular cleaning (human, robotic, or automated), using methods such as water washes, brushes, and electrodynamic cleaning systems.

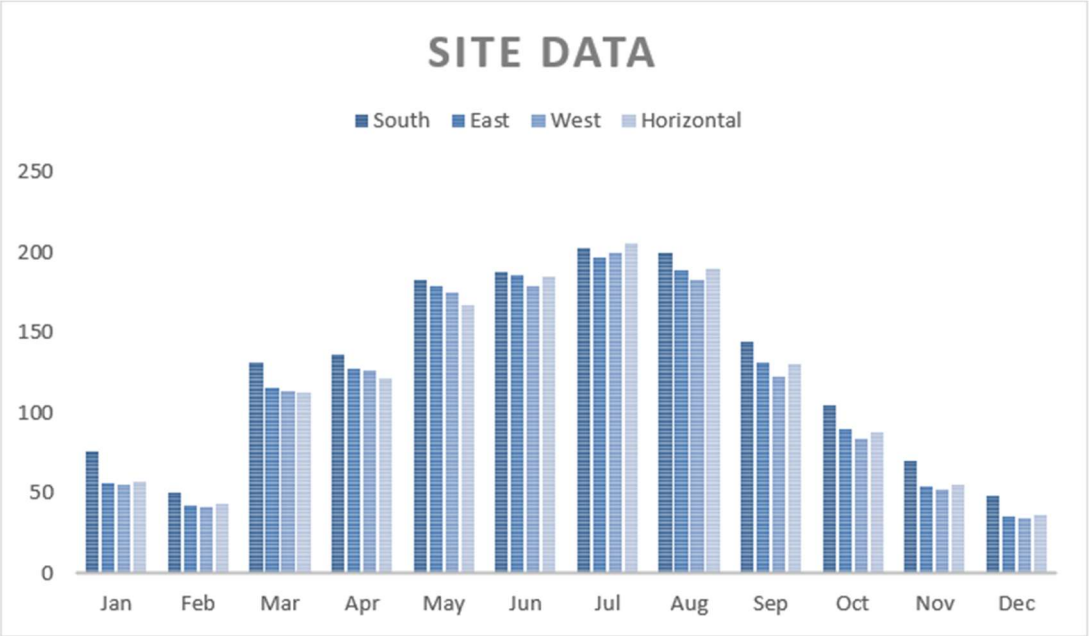

Figure 4.13. Site data.

In our PV roof system, the tilt angle of the panels has a considerable impact on decreasing the soiling effect. Horizontal panels tend to collect more dust and have a slower snow-melting rate, increasing the amount of work necessary to clean. In contrast, panels set at an appropriate tilt angle require less care, especially as Sakarya sees heavy rains from November to May, which naturally helps keep the panels cleaner. However, during the summer, all panels require a regular cleaning routine to reduce the impacts of soiling. The last figure shows a comparison chart between south, east, west, and horizontal panels based on data collected from the real site. An interesting point is that east and west-facing panels produce energy values very close to those of the horizontal panels, and in some months, they even generate more energy. This suggests that tilting panels toward the east or west can be a better than horizontal choice due to less cost and maintaining efforts (periodic cleaning) that tilted panels need. Additionally, energy production can be further improved by tilting the east and west-facing panels at an angle of 8° to 9°, as recommended by PV*SOL simulations.

5. CONCLUSION AND RECOMMENDATIONS

This study shows how much the tilt angle of solar panels affects power output and considers the soiling effect. MATLAB was used to develop a new model for diffuse solar radiation. The developed model was used to estimate total solar radiation on tilted surfaces and to find the best tilt angles for the rooftop PV system at the Faculty of Electrical and Electronics Engineering. The calculated optimum yearly tilt angle for south-facing panels is 32.64°. PVSOL software simulations provided a similar result, suggesting an optimum tilt angle of 32° south.

The PV*SOL software also helped determine the system's energy production. The system is expected to export around 5660 kWh per year to the grid. South-facing panels produce the most energy at 1632.5 kWh/year. Horizontal panels follow with 1421.2 kWh/year, then east-facing panels with 1371.9 kWh/year, and west-facing panels with the lowest value at 1234.6 kWh/year. The optimum tilt angle changes throughout the year, from 0.1° in June to 60.42° in December. Based on these results, the recommended tilt angles are 32° for south facing panels, and 8° to 9° for east and west-facing panels.

The soiling effect can greatly reduce panel efficiency. Heavy rain and snow in Sakarya from November to May help clean the panels naturally with little human effort. However, from June to October, there is less rain, so dirt builds up more quickly. It is recommended to clean tilted panels twice per month during the summer and to clean horizontal panels weekly since they collect more dust and do not self-clean easily.

The comparison between PV*SOL simulation results and real site measurements shows a similar pattern throughout the year. The smallest errors appear in May and June with about 0.34% difference, showing very close agreement. The largest differences occur in February with a 52.13% error and in December with a 29.94% error. The highest energy production happens in summer months like June, July, and August, which is expected due to stronger sunlight. Overall, PV*SOL provides reliable results with a total error of just 0.68%. A comparison between south, east, west, and horizontal panels based on real site data shows that east and west-facing panels can

produce similar energy to horizontal panels. In some months, east and west-facing panels can even produce more than horizontal panels. This means east or west-facing panels with a small tilt like 8° to 9° as PV*SOL suggested or even the east and west site facing panels in the site can be a better choice than flat ones, as they need less cleaning efforts and cost less to maintain.

Additional simulations were done to check how fully covered rooftop PV systems can work for each direction: south, east, west, and horizontal. The results showed that the south side can hold 59 panels, the east side can hold 63 panels, the west side can hold 60 panels, and the horizontal surface can also hold 60 panels. Even though the south side has the fewest panels, it gives the highest energy production of about 31,101 kWh per year. The horizontal system produces about 28,560 kWh per year, the east system about 27,722 kWh per year, and the west system about 23,676 kWh per year. Cost is an important factor. Tilted panels generally cost more to install because they need extra equipment and more effort, even though fewer panels are used. Horizontal panels are cheaper and easier to install but need more cleaning to keep them working well.

The tilt angle not only helps to improve energy production but also reduces the soiling effect. Horizontal panels collect more dust and have low snow-melting rate, making cleaning harder, while tilted panels stay cleaner, especially during the rainy season. Still, all panels need regular cleaning during the year to keep them efficient. In general, south-facing panels are recommended because they provide higher efficiency that can justify their cost compared to horizontal or east and west-facing panels. For buildings with tilted roofs, site data showed that horizontal panels have energy production values close to east and west-facing panels.

Also, in the case of flat-roof buildings, installing east and west-facing panels remains a good option, as they offer energy production close to both horizontal and south facing tilted panels. Additionally, east and west-facing panels typically have lower cleaning costs, which presents a long-term advantage.

REFERENCES

[1] U.S. Department of Energy. (n.d.). Top 6 things you didn't know about solar energy. Retrieved May 17, 2025, from https://www.energy.gov/articles/top-6-things-you-didnt-know-about-solar-energy

[2] International Renewable Energy Agency. (2024). Renewable power generation costs in 2023. International Renewable Energy Agency. https://www.irena.org/publications

[3] Lameirinhas, R. A. M., Torres, J. P. N., & Dias, J. P. da M. C. (2022). Multi-junction solar cells efficiency under real operating conditions: A review. Energies, 15(18), 6492. https://doi.org/10.3390/en15186492

[4] U.S. Department of Energy. (n.d.). Solar energy. Retrieved May 17, 2025, from https://www.energy.gov/topics/solar

[5] Duarte, F., Torres, J. P. N., Baptista, A., & Marques Lameirinhas, R. A. (2021). Optical nanoantennas for photovoltaic applications. Nanomaterials, 11(2), 422. https://doi.org/10.3390/nano11020422

[6] Boerema, N., Morrison, G., Taylor, R., & Rosengarten, G. (2013). High temperature solar thermal central-receiver billboard design. Solar Energy, 97, 356–368. https://doi.org/10.1016/j.solener.2013.09.008

[7] Law, E. W., Prasad, A. A., Kay, M., & Taylor, R. A. (2014). Direct normal irradiance forecasting and its application to concentrated solar thermal output forecasting A review. Solar Energy, 108, 287–307. https://doi.org/10.1016/j.solener.2014.07.008

[8] Philipps, S., & Warmuth, W. (2024). Photovoltaics Report. Fraunhofer Institute for Solar Energy Systems ISE. https://www.ise.fraunhofer.de

[9] National Renewable Energy Laboratory. (2025). Best Research-Cell Efficiency Chart. Retrieved from https://www.nrel.gov/pv/cell-efficiency.html

[10] Abou-Ras, D., Wagner, S., Stanbery, B. J., Schock, H.-W., Scheer, R., Stolt, L., Siebentritt, S., Lincot, D., Eberspacher, C., Kushiya, K., & Tiwari, A. N. (2017). Innovation Highway: Breakthrough milestones and key developments in chalcopyrite photovoltaics from a retrospective viewpoint. Thin Solid Films, 633, 2–20. https://doi.org/10.1016/j.tsf.2017.01.005

[11] Shay, J. L., Wagner, S., & Kasper, H. M. (1975). Efficient $CuInSe_2$/CdS solar cells. Applied Physics Letters, 27(2), 89–91. https://doi.org/10.1063/1.88372

[12] Martí, A., & Araújo, G. L. (1996). Limiting efficiencies for photovoltaic energy conversion in multigap systems. Solar Energy Materials and Solar Cells, 43, 203–222. https://doi.org/10.1016/0927-0248(96)00015-3

[13] Werner, J., Niesen, B., & Ballif, C. (2018). Perovskite/silicon tandem solar cells: Marriage of convenience or true love story? An overview. Advanced Materials Interfaces, 5(1), 1700731. https://doi.org/10.1002/admi.201700731

[14] Taşdemiroğlu, E., & Sever, R. (1991). Estimation of monthly average daily horizontal diffuse radiation in Turkey. Energy, 16(4), 787–790. https://doi.org/10.1016/0360-5442(91)90030-P

[15] Barbaro, S., Cannata, G., Coppolino, S., Leone, C., & Sinagra, E. (1981). Diffuse solar radiation statistics for Italy. Solar Energy, 26(5), 429–435. https://doi.org/10.1016/0038-092X(81)90222-X

[16] Kaygusuz, K., & Ayhan, T. (1999). Analysis of solar radiation data for Trabzon, Turkey. Energy Conversion and Management, 40(5–6), 545–556. https://doi.org/10.1016/S0196-8904(98)00119-8

[17] Aras, H., Balli, O., & Hepbasli, A. (2006). Estimating monthly mean daily diffuse solar radiation by artificial neural networks and regression methods in Turkey. Energy Conversion and Management, 47(15–16), 2240–2249. https://doi.org/10.1016/j.enconman.2005.11.024

[18] Elhadidy, M. A., & Abdel-Nabi, D. Y. (1991). Diffuse fraction of daily global radiation at Dhahran, Saudi Arabia. Solar Energy, 46(2), 89–95. https://doi.org/10.1016/0038-092X(91)90020-W

[19] Jain, P. C. (1990). A model for diffuse and global irradiation on horizontal surfaces. Solar Energy, 45(5), 301–308. https://doi.org/10.1016/0038-092X(90)90015-5

[20] Tarhan, S., & Sari, A. (2005). Model selection for global and diffuse radiation over the Central Black Sea (CBS) region of Turkey. Energy Conversion and Management, 46(4), 605–613. https://doi.org/10.1016/j.enconman.2004.04.004

[21] Liu, B. Y. H., & Jordan, R. C. (1960). The interrelationship and characteristic distribution of direct, diffuse, and total solar radiation. Solar Energy, 4(3), 1–19. https://doi.org/10.1016/0038-092X(60)90062-1

[22] Erbs, D. G., Klein, S. A., & Duffie, J. A. (1982). Estimation of the diffuse radiation fraction for hourly, daily, and monthly-average global radiation. Solar Energy, 28(4), 293–302. https://doi.org/10.1016/0038-092X(82)90302-4

[23] Ulgen, K., & Hepbasli, A. (2002). Comparison of solar radiation correlations for Izmir, Turkey. International Journal of Energy Research, 26(5), 413–430. https://doi.org/10.1002/er.794

[24] Yu, Y., Wang, L., & Zhang, X. (2023). Adaptive Liu & Jordan-type models for estimating hourly diffuse solar irradiation: A case study in China. Energy Conversion and Management, 293, 117455. https://doi.org/10.1016/j.enconman.2023.117455

[25] Yu, Y., Wang, L., & Zhang, X. (2023). Adaptive Liu & Jordan-type models for estimating hourly diffuse solar irradiation: A case study in China. Energy Conversion and Management, 293, 117455. https://doi.org/10.1016/j.enconman.2023.117455

[26] Tiris, M., Tiris, Ç., & Türe, I. E. (1996). Correlations of monthly-average daily global, diffuse and beam radiations with hours of bright sunshine in Gebze, Turkey. Energy Conversion and Management, 37(9), 1417–1421. https://doi.org/10.1016/0196-8904(95)00227-8

[27] Lingamgunta, C., & Veziroğlu, T. N. (2004). A universal relationship for estimating clear sky insolation. Energy Conversion and Management, 45(1), 27–52. https://doi.org/10.1016/S0196-8904(03)00111-0

[28] Aksoy, B. (1997). Estimated monthly average global radiation for Turkey and its comparison with observations. Renewable Energy, 10(4), 625–633. https://doi.org/10.1016/S0960-1481(96)00035-3

[29] Muneer, T., & Munawwar, S. (2006). Potential for improvement in estimation of solar diffuse irradiance. Energy Conversion and Management, 47(1–2), 68–86. https://doi.org/10.1016/j.enconman.2005.03.015

[30] Dincer, I. (2000). Renewable energy and sustainable development: A crucial review. Renewable and Sustainable Energy Reviews, 4(2), 157–175. https://doi.org/10.1016/S1364-0321(99)00011-8

[31] Ideriah, F. J. K. (1981). A model for calculating direct and diffuse solar radiation. Solar Energy, 26(5), 447–452. https://doi.org/10.1016/0038-092X(81)90224-3

[32] Klein, S. A. (1977). Calculation of monthly average insolation on tilted surfaces. Solar Energy, 19(4), 325–329. https://doi.org/10.1016/0038-092X(77)90001-9

[33] Xu, R., Ni, K., Hu, Y., Si, J., Wen, H., & Yu, D. (2017). Analysis of the optimum tilt angle for a soiled PV panel. Energy Conversion and Management, 148, 100–109. https://doi.org/10.1016/j.enconman.2017.05.058

[34] Abdeen, E., Orabi, M., & Hasaneen, E. S. (2017). Optimum tilt angle for photovoltaic system in desert environment. Solar Energy, 155, 267–280. https://doi.org/10.1016/j.solener.2017.06.031

[35] Aksoy Tırmıkçı, C., & Yavuz, C. (2018). Determining optimum tilt angles of solar surfaces in Sakarya, Turkey. Theoretical and Applied Climatology, 133(1–2), 15–22. https://doi.org/10.1007/s00704-017-2174-x

[36] U.S. Department of Energy. (n.d.). Solar radiation basics. Office of Energy Efficiency & Renewable Energy. Retrieved May 17, 2025, from https://www.energy.gov/eere/solar/solar-radiation-basics

[37] NASA. (n.d.). What is the sun's role in climate change? NASA Science. Retrieved May 17, 2025, from https://science.nasa.gov/earth/climate-change/what-is-the-suns-role-in-climate-change

[38] Janssen, P. J. D., Lambreva, M. D., Plumeré, N., Bartolucci, C., Antonacci, A., Buonasera, K., Frese, R. N., Scognamiglio, V., & Rea, G. (2014). Photosynthesis at the forefront of a sustainable life. Frontiers in Chemistry, 2, 36. https://doi.org/10.3389/fchem.2014.00036

[39] World Meteorological Organization. (n.d.). The sun's impact on the Earth. Retrieved May 17, 2025, from https://wmo.int/suns-impact-earth

[40] Lindsey, R. (2009, January 14). Climate and Earth's energy budget. NASA Earth Observatory. Retrieved May 17, 2025, from https://earthobservatory.nasa.gov/features/EnergyBalance

[41] NASA Goddard Space Flight Center. (n.d.). Solar irradiance. Sun Climate. Retrieved May 17, 2025, from https://sunclimate.gsfc.nasa.gov/article/solar-irradiance

[42] Science Photo Library. (n.d.). Electromagnetic spectrum illustration. Retrieved May 17, 2025, from https://www.sciencephoto.com/media/705287/view/electromagnetic-spectrum-illustration

[43] NASA Earth Observatory. (n.d.). Earth's energy balance. Retrieved May 17, 2025, from https://earthobservatory.nasa.gov/features/SORCE/sorce_02.php

[44] Raja, D. (2019, December 2). Solar radiation measurement methods using pyrheliometer and pyranometer. Circuit Digest. Retrieved May 17, 2025, from https://circuitdigest.com/tutorial/solar-radiation-measurement-methods-using-pyrheliometer-and-pyranometer

[45] Oliveira, M., Silva Lopes, H., Mendonça, P., Tenpierik, M., & Torres Silva, L. (2024). Solar radiation measurement tools and their impact on in situ testing: A Portuguese case study. Buildings, 14(7), 2117. https://doi.org/10.3390/buildings14072117

[46] Aksoy, B. (2011). Solar radiation over Turkey and its analysis. International Journal of Remote Sensing. Advance online publication. https://doi.org/10.1080/01431161.2010.508056

[47] de Souza, M. B., Tonolo, É. A., Yang, R. L., Tiepolo, G. M., & Urbanetz Junior, J. (2019). Determination of diffused irradiation from horizontal global irradiation: Study for the city of Curitiba. Brazilian Archives of Biology and Technology, F62(spe), e19190014. https://doi.org/10.1590/1678-4324-smart-2019190014

[48] T.C. Enerji ve Tabii Kaynaklar Bakanlığı. (n.d.). Sakarya iline ait güneş enerjisi verileri. Güneş Enerjisi Potansiyeli Atlası. Retrieved May 17, 2025, from https://gepa.enerji.gov.tr/pages/54.aspx

[49] Page, J. K. (1961). The estimation of monthly mean values of daily total short wave radiation on vertical and inclined surfaces from sunshine records for latitudes 40°N–40°S. Proceedings of the United Nations Conference on New Sources of Energy, 4(598), 378–390.

[50] Gopinathan, K. K. (1988). Computing the monthly mean daily diffuse radiation from clearness index and percent possible sunshine. Solar Energy, 41(4), 379–385. https://doi.org/10.1016/0038-092X(88)90034-5

[51] Khorasanizadeh, H., Mohammadi, K., & Mostafaeipour, A. (2014). Establishing a diffuse solar radiation model for determining the optimum tilt angle of solar surfaces in Tabass, Iran. Energy Conversion and Management, 78, 805–814. https://doi.org/10.1016/j.enconman.2013.11.048

[52] Bessa, J. G., Micheli, L., Almonacid, F., & Fernández, E. F. (2021). Monitoring photovoltaic soiling: Assessment, challenges, and perspectives of current and potential strategies. iScience, 24, 102165. https://doi.org/10.1016/j.isci.2021.102165

[53] Li, X., Mauzerall, D. L., & Bergin, M. H. (2020). Global reduction of solar power generation efficiency due to aerosols and panel soiling. Nature Sustainability, 3(9), 720–727. https://doi.org/10.1038/s41893-020-0553-

[54] Fernández Solas, Á., Riedel Lyngskær, N., Hanrieder, N., Norde Santos, F., Wilbert, S., Nygard Riise, H., Polo, J., Fernández, E. F., Almonacid, F., Talavera, D. L., & Micheli, L. (2025). Photovoltaic soiling loss in Europe: Geographical distribution and cleaning recommendations. Renewable Energy, 239, 122086. https://doi.org/10.1016/j.renene.2024.122086

[55] Erduman, A., Durusu, A., Kilickiran, H. C., Kekezoglu, B., & Tanrioven, M. (2016, August 28–31). The effect of soiling factor on PV array performance: A case study for Istanbul. European Conference on Renewable Energy Systems, Istanbul, Turkey.

CURRICULUM VITAE

Name Surname : ABDALAZIZ TAREK ABDALAZIZ RAGAB

EDUCATION:

- **Undergraduate** : 2022, Muğla Sıtkı Koçman Üniversitesi, Engineering, Electrical and Electronics Engineering

PUBLICATIONS, PRESENTATIONS AND PATENTS ON THE THESIS:

- Ragab A., Yavuz C., (2025, 16-17, March). Define New Diffuse Solar Radiation Equation Model In Sakarya. *International science And Art Research Center - Uluslararası Selçuk Bilimsel Araştırmalar Kongresi Management*